A physically based parameterization of gravity drainage for sea-ice modelling

David W. Rees Jones[1,2] and M. Grae Worster[1]

Abstract. We incorporate a physically derived parameterization of gravity drainage, in terms of a convective upwelling velocity, into a one-dimensional, thermodynamic sea-ice model of the kind currently used in coupled climate models. Our parameterization uses a local Rayleigh number to represent the important feedback between ice salinity, porosity, permeability and desalination rate. It allows us to determine salt fluxes from sea ice and the corresponding evolution of the bulk salinity of the ice, in contrast to older, established models that prescribe the ice salinity. This improves the predictive power of climate models in terms of buoyancy fluxes to the polar oceans, and also the thermal properties of sea ice, which depend on its salinity. We analyze the behaviour of existing fixed-salinity models, elucidate the physics by which changing salinity affects ice growth and compare against our dynamic-salinity model, both in terms of laboratory experiments and also deep-ocean calculations. These comparisons explain why the direct effect of ice salinity on growth is relatively small (though not always negligible, and sometimes different from previous studies), and also highlight substantial differences in the qualitative pattern and quantitative magnitude of salt fluxes into the polar oceans. Our study is particularly relevant to growing first-year ice, when gravity drainage is the dominant mechanism by which ice desalinates. We expect that our dynamic model, which respects the underlying physics of brine drainage, should be more robust to changes in polar climate and more responsive to rapid changes in oceanic and atmospheric forcing.

Citation: Rees Jones, D. W., and M. G. Worster (2014), A physically based parameterization of gravity drainage for sea-ice modeling, J. Geophys. Res. Oceans, 119, 55995621, doi:10.1002/2013JC009296. An edited version of this paper was published by AGU. Copyright (2014) American Geophysical Union.

1. Introduction

1.1. Sea ice in coupled climate models

Sea ice forms a dynamic interface between the ocean and atmosphere and so constitutes an integral aspect of any coupled climate model [*Gent*, 2012]. Although only a few meters thick, sea ice plays a significant role in the coupling between ocean and atmosphere because it reflects a higher proportion of solar radiation than open water, insulates the polar oceans, and stores latent heat [reviewed in *Weeks*, 2010]. As well as these thermal considerations, sea ice has important implications for the transport of salt in the polar regions. Sea ice grows as a porous matrix in which salty brine is held in the interstices of the ice. Thus it is a mushy layer [*Feltham et al.*, 2006]. The seasonal desalination of sea ice is a crucial salt flux for the polar oceans, comparable to the (negative) salt fluxes from rivers and ice-sheet melting, and drives vertical mixing of the upper layer of the ocean. The surface salt flux from sea ice has been measured to be as high as 1–2 kg/m^2/day for new ice [*Notz and Worster*, 2008]. Salt fluxes are known to be sensitive to short-term changes in the external forcing [*Widell et al.*, 2006; *Jardon et al.*, 2013]. Consequently, the representation of salt fluxes significantly affects the salinity structure of the ocean in climate models [*Vancoppenolle et al.*, 2005, 2009b].

Within coupled climate models, sea ice is typically accounted for by using a small modeling component that is coupled to ocean and atmosphere models. The sea-ice component accounts for the thermodynamic growth and melting of ice, the movement of ice due to wind stress, its response to internal stresses, lateral melting and the formation of pressure ridges [*e.g. Hunke and Lipscomb*, 2008; *Vancoppenolle et al.*, 2009a, b]. In this article, we restrict attention to the thermodynamic growth of ice and analyze a one-dimensional, thermodynamic model of ice growth that calculates the change of an ice-thickness distribution. Thermodynamic growth accounts for much of the change at the thin-ice end of this distribution, which is particularly important for salt fluxes, as these are much greater for thinner ice. The dynamic-salinity model we introduce is structurally similar to fixed-salinity models currently used in many coupled climate models. Fixed-salinity models solve a heat equation in which the thermal properties of ice, its heat capacity and conductivity, depend on the temperature and salinity of the ice. They are deficient in that, while the temperature is determined as part of the solution, the salinity field is prescribed. By contrast, in our new model (as well as in the other new models discussed below), the salinity is determined dynamically.

There has been much recent interest in determining the salinity of sea ice dynamically. Some studies are at a small scale and resolve gravity drainage in two-dimensional numerical simulations [*Oertling and Watts*, 2004; *Wells et al.*, 2011]. Other studies are at the polar-ocean scale and parameterize gravity drainage [*Vancoppenolle et al.*, 2009b, 2010;

[1]Institute of Theoretical Geophysics, Department of Applied Mathematics and Theoretical Physics, University of Cambridge, Cambridge, UK

[2]Atmospheric, Oceanic and Planetary Physics, Department of Physics, University of Oxford, Oxford, UK

0148-0227/15/$9.00

Jeffery et al., 2011; *Saenz and Arrigo*, 2012; *Turner et al.*, 2013; *Griewank and Notz*, 2013]. Their parameterizations variously involve, sometimes in combination, relaxation of the salinity profile, enhanced molecular diffusion, mixing length diffusion, empirical formulae based on *Cox and Weeks* [1988], and a local Rayleigh number. Our approach is to take a simple theoretical model of gravity drainage in terms of a Rayleigh number derived from small scale models [*Rees Jones and Worster*, 2013a, b], and cast it in a form appropriate to these large scale models. Our model can be considered one of a new generation of dynamic-salinity sea-ice models and is most similar to *Turner et al.* [2013] and *Griewank and Notz* [2013]. We discuss how our model compares to those two models in section 2.3.

In section 2, we develop our model starting with the phase-averaged mushy-layer equations for heat and salt conservation in one spatial dimension. In the case of non-convecting sea ice, *Feltham et al.* [2006] have shown that these equations are essentially equivalent to those used in generations of models derived from the fundamental description given by *Maykut and Untersteiner* [1971], including *Bitz and Lipscomb* [1999] which is used in CICE: the Los Alamos Sea Ice Model [*Hunke and Lipscomb*, 2008]. Our model develops these further by determining a convecting upwelling velocity internal to the sea ice.

1.2. Desalination of sea ice: modeling gravity drainage

A number of different mechanisms lead to the desalination of sea ice observed over time in field measurements [*Nakawo and Sinha*, 1981; *Eicken*, 1992]. *Untersteiner* [1968] reviewed and estimated the strength of brine-pocket migration, brine expulsion, flushing and gravity drainage. Brine-pocket migration [*Whitman*, 1926], in which the temperature gradient establishes an interstitial salinity gradient down which salt diffuses, is very slow and accounts for little salt transport, so we neglect it in this article. Brine expulsion [*Bennington*, 1963], caused by the smaller density of solid ice compared to liquid water, redistributes salt within the ice. However, this mechanism causes no net salt flux from ice to the ocean [*Notz and Worster*, 2009] and our study strongly suggests that it would have only a marginal influence on ice growth rate (see section 4.3). Flushing by meltwater that ponds on the surface of the ice, the magnitude of which is estimated by *Untersteiner* [1968] and analyzed in terms of Darcy flow by *Eicken et al.* [2004], is very significant in the summer when water from melt ponds can lead to rapid desalination of ice. But here we focus on gravity drainage [*Eide and Martin*, 1975; *Cox and Weeks*, 1975], which is a convective process caused by density gradients dominated by vertical salinity variations in the interstitial brine, established as the interstitial brine becomes increasingly saline as the ice continues to solidify. It is the dominant process of salt release while ice grows during the winter [*Notz and Worster*, 2009].

We base our modelling approach on a recently developed Channel-Active-Passive (CAP) model [*Rees Jones and Worster*, 2013a, b] in which we divide up a section of sea ice into a brine channel, an active region where horizontal density gradients sustain a convective flow, and a passive region that is horizontally uniform. The CAP model allows us to parametrize the convective upwelling velocity in a way that captures the underlying physics, using a Rayleigh number to represent the relative strength of the interstitial salinity gradient that drives convection and the effects of viscous dissipation, which depends on the permeability of sea ice. The vertical structure of the convective upwelling is determined as part of the solution. The CAP model includes the flow and viscous dissipation in the brine channel, and in this aspect is more complete than, for example, *Turner et al.* [2013] in that it determines rather than prescribes the channel width, which depends on the strength of convection. The interstitial brine is relatively saline compared with the ocean, so the convective upwelling amounts to a net freshening. This is balanced by downward flow in the brine channels and results in brine fluxes into the ocean. Two parameters in our model – a critical Rayleigh number and a proportionality constant between upwelling velocity and effective Rayleigh number – have been calculated in idealized situations [*e.g. Wells et al.*, 2010, 2013; *Rees Jones and Worster*, 2013a]. However, in this paper, we treat them as tuning parameters that we adjust to describe the laboratory experiments of *Wettlaufer et al.* [1997] and *Notz* [2005].

Convection is sometimes confined to a layer at the bottom of sea ice. For example, *Eide and Martin* [1975] observed dye being 'entrained' into the ice, an observation that we attribute to convection. That the dye height tends to a maximum less than the total thickness of the ice (evident from the exponential fits in the original paper and interpreted in *Rees Jones and Worster* [2013b]) points to convection being confined. Confinement of convection arises where there is insufficient gravitational potential energy within the compositional density gradient to overcome thermal diffusion and viscous dissipation. This competition can be described by a mush Rayleigh number: the upper part of the mushy layer has a Rayleigh number below the critical value required for convection and so is stagnant, whereas the lower part of the mushy layer has a Rayleigh number above the critical value and so convects. The brine in the stagnant layer is not necessarily 'trapped' in the sense of the ice being impermeable. Indeed, the permeability of sea ice remains a major open question [*Freitag*, 1999; *Petrich et al.*, 2006; *Golden et al.*, 2007] to which we return in section 5. There we apply our model to a wide range of problems in order to analyze indirectly the relationship between the porosity and permeability of sea ice, highlighting the distinction between local and bulk permeability.

It is now well established that a Rayleigh number governs the onset and strength of convection in mushy layers such as sea ice [*Worster*, 1992, 1997] and so we propose using a *local* Rayleigh number to determine the thickness of the convecting layer, as suggested by *Notz and Worster* [2008]. In sea ice, strongly varying permeability is responsible for the confinement of convection. In other physical systems, the mechanism can differ. For example, in experiments analogous to sea ice but using sugar instead of salt [*Aussillous et al.*, 2006] and in the 'stagnant-lid' mode of convection in magma chambers [*Davaille and Jaupart*, 1993], confinement is thought to be caused by the strong variation of viscosity with temperature. Our approach here, which is based on fundamental physical principles, should be generalizable to such systems.

In principle, the parameterized convective upwelling velocity could also be used to calculate the transport of nutrients and trace gases in climate models [*Vancoppenolle et al.*, 2010]. In order to test the predictive ability of our model in terms of sea-ice growth and salt fluxes, we compare its results with measurements from laboratory experiments in section 3. We discuss the implications of our parameterization for climate modelers in section 4 by analysing the behaviour of a fixed-salinity model in comparison with our dynamical-salinity model, both theoretically and by applying them to a range of scenarios.

2. Formulating a one-dimensional model of sea ice

2.1. Model configuration

We consider ice grown from an upper cold plate of temperature $T_B(t)$, as shown in figure 1. This configuration allows

for comparison with experiments. Our model dynamically evolves the internal temperature T and bulk salinity S of the ice using a parameterized vertical Darcy velocity w. It is important to note that the bulk salinity is always less than the interstitial salinity C (which is often called the brine salinity), which is not an independent variable but coupled to T through the liquidus relation $C = C_L(T)$, since sea ice can be assumed to be at local thermodynamic equilibrium internally [*Feltham et al.*, 2006]. We use $T = T_L(C)$ for the inverse of this relationship. The salinities S and C are related through the solid fraction ϕ by

$$S = (1-\phi)C + \phi C_s \approx (1-\phi)C, \tag{1}$$

given that the salinity of solid ice $C_s \approx 0$. We rearrange equation (1) to determine the solid fraction

$$\phi(T,S) = 1 - S/C_L(T). \tag{2}$$

Sea ice of thickness $h(t)$ grows into a tank of fixed depth H. We take the purely liquid region in the tank (which in this paper we refer to as the 'ocean') to be well mixed, owing to thermal and compositional convective mixing, having temperature $T_l(t)$ and salinity $C_l(t)$. This treatment of the ocean is approximate but is appropriate for this study as it is not part of the sea-ice component of a coupled climate model.

2.2. Model equations

Sea ice is a multiphase, reactive porous medium and so is an example of a wider class of systems called mushy layers [*Worster*, 2000; *Feltham et al.*, 2006; *Hunke et al.*, 2011]. The mushy-layer equations for heat and salt conservation in one spatial dimension can be used to derive our model equations, generalizing *Feltham et al.* [2006],

$$c_i \frac{\partial T}{\partial t} + c_w w \frac{\partial T}{\partial z} = \frac{\partial}{\partial z}\left(k_i \frac{\partial T}{\partial z}\right), \tag{3}$$

$$\frac{\partial S}{\partial t} = -w \frac{\partial C}{\partial z}, \tag{4}$$

in which the major novelty is that we determine a convective Darcy velocity w due to gravity drainage based on the CAP model discussed in section 1.2

$$w = \begin{cases} -\alpha Ra_e \dfrac{k_l}{c_l} \dfrac{z - z_c}{(h - z_c)^2} & \text{if } z \geq z_c \\ 0 & \text{if } z < z_c \end{cases} \tag{5}$$

where α is a dimensionless prefactor [*Rees Jones and Worster*, 2013a, b], Ra_e is an effective Rayleigh number and z_c is the position of the top of the convecting layer determined in section 2.3 (*cf.* figure 1). Since we focus on gravity drainage, we neglect diffusion of salt in (4), which is small, and also brine expulsion.

Effective volumetric heat capacities c_i and c_w of sea ice and brine transport respectively are determined (see appendix A for details) by averaging over the two phases and accounting for the latent heat of fusion L per unit volume of solid formed at 0°C. In this, we generalize the 'classical' expression [*Malmgren*, 1927] to a nonlinear liquidus. We neglect the difference between the heat capacities of the solid and liquid phases (which is equivalent to a temperature-dependent latent heat) and the heat of solution, as these are both small (together they amount to about 1% of the latent heat of sea ice, see *Notz* [2005] for details). Thus

$$c_i(T,S) = c_s - LSC_L' C_L^{-2}, \tag{6}$$

$$c_w(T,S) = c_l - \frac{LC_L'}{C_L}, \tag{7}$$

where C_L' denotes the derivative of C_L with respect to T, and subscripts s and l represent properties of solid and liquid phase respectively. We use a cubic fit for the liquidus salinity of NaCl [*Weast*, 1971]

$$C_L(T) = -17.6T - 0.389T^2 - 0.00362T^3. \tag{8}$$

For natural sea ice, a fit to the data of *Assur* [1958] could be used [*Notz*, 2005].

Likewise, the thermal conductivity of sea ice [*Ono*, 1968; *Batchelor*, 1974]

$$k_i(T,S) = k_s - (k_s - k_l)\, SC_L^{-1}. \tag{9}$$

Throughout this article, we take parameter values, named and listed in table 1, appropriate to the solidification of aqueous sodium chloride (NaCl), since it is the most abundant salt in seawater and allows direct comparison with the laboratory experiments discussed in section 3.1.

2.3. Parameterization of convective velocity w: applying the CAP model

The key novelty in our model is that we determine the convective velocity w dynamically from a simple physical parameterization. In *Rees Jones and Worster* [2013b], we applied a steady-state CAP model of mushy-layer convection in two or three dimensions [*Rees Jones and Worster*, 2013a] to transient sea-ice growth, which we now apply to a one-dimensional model as follows.

The thickness of the convecting layer and the strength of convection are set by a depth-dependent *local* Rayleigh number introduced in section 1.2 [*cf. Notz and Worster*, 2008; *Vancoppenolle et al.*, 2010; *Griewank and Notz*, 2013]

$$Ra(z) = \frac{c_l g \beta}{k_l \nu} \left[C_L(T(z)) - C_L(T_l)\right](h - z)K(z), \tag{10}$$

based on the ratio of the potential energy difference from a height z to the ice–ocean interface h relative to the thermal diffusion and the viscous dissipation caused by the flow required to replace the fluid that moves into the ocean. When this ratio is sufficiently large, there is enough potential energy for convection to occur. Note that the ratio of an advective to a diffusive timescale discussed in *Griewank and Notz* [2013] is better thought of as Péclet number, which is itself a function of the Rayleigh number.

We take the harmonic mean permeability

$$K(z) = K_0 \left[\frac{1}{h - z}\int_z^h \frac{1}{K_l(\phi(z'))}\, dz'\right]^{-1}, \tag{11}$$

where K_0 is a dimensional constant (see table 1) and $K_l(\phi) = (1-\phi)^3$ is a dimensionless local relationship between porosity and permeability. The latter was suggested by *Worster* [1992] as a simplified form of the Kozeny porosity–permeability relationship and used by various subsequent studies of convection in a mushy layer [*e.g. Amberg and Homsy*, 1993; *Schulze and Worster*, 1998; *Chung and Worster*, 2002; *Wells et al.*, 2010, 2013]. The harmonic mean in equation (11) reduces to $K = K_0(1-\phi)^3$ if ϕ is constant, which is approximately the same as the experimental fit to measurements of *Freitag* [1999], and is appropriate in that it is the bulk permeability of a series of layers of varying permeability [*Phillips*, 1991], on the assumption that the flow is dominantly vertical. This measure appropriately accounts for the fact that a fluid parcel being replaced at the top of the mushy layer requires a flow through all the

layers beneath it. Note that *Notz and Worster* [2008] and *Vancoppenolle et al.* [2010] take $K(z)$ to correspond to the least-permeable layer between height z and the ice–ocean interface, which is comparable since the harmonic mean is dominated by the least permeable region. From a computational perspective, their suggestion has the potential disadvantage of behaving very non-locally. However, we acknowledge that our proposal (equation 11) is only tentative. The uncertainty arises from difficulties in making direct measurements of permeability, and we discuss recent suggestions and our own contribution in section 5.

The local Rayleigh number defined by equation (10) is used to determine both the region of convection (figures 1 & 2) and also an effective Rayleigh number governing the strength of convection in equation (5) as follows. If $Ra(z)$ is everywhere less than a critical value R_c (figure $2a$), there is no convecting layer and $Ra_e = 0$. Otherwise, there is convection in the region between the ice–ocean interface $z = h$ and some critical depth $z = z_c$, which we determine as follows. If $Ra(0) \geq R_c$, then the whole mushy layer convects ($z_c = 0$, figure $2c,d$). Otherwise, if $Ra(0) < R_c$, there is a first point z_c such that $Ra(z_c) = R_c$ (figure $2b$). A fluid parcel at this depth has enough potential energy to convect through the whole depth below it $z_c \leq z \leq h$, being replaced by fluid rising up through the rest of the layer.

Finally, motivated by *Wells et al.* [2010, 2011, 2013], we define an effective Rayleigh number in terms of the degree of supercriticality,

$$Ra_e = \max_{z_c \leq z \leq h} Ra(z) - R_c, \tag{12}$$

as marked in figure $2b$. Other parameterizations are possible; in particular, we investigated both confining convection in the case of figure $2c$ and also letting

$$Ra_e = \max_{z_c \leq z \leq h} Ra(z), \tag{13}$$

which shares with (12) the property that flux is proportional to Rayleigh number at large Rayleigh number [*Wells et al.*, 2010, 2013; *Rees Jones and Worster*, 2013a] but found that these parameterizations were less satisfactory.

Independently, *Turner et al.* [2013] and *Griewank and Notz* [2013] have developed advective parameterizations of gravity drainage that involve a Rayleigh number. As discussed in section 1.2, these are the most similar to our own of the new generation of models. For example, the recently proposed diffusive parameterizations of *Vancoppenolle et al.* [2010] and *Jeffery et al.* [2011] differ more substantially and we discuss these in *Rees Jones and Worster* [2013b]. Here we focus on the several important respects in which our model differs. Our single instantaneous effective Rayleigh number captures the non-local nature of convection arguably better than the more local 'rapid mode of gravity drainage' in *Turner et al.* [2013] and 'convective' parameterization in *Griewank and Notz* [2013], since it applies to the whole flow and means that the velocity at a given depth is related to the velocity everywhere within the convecting layer, consistent with the detailed calculations from which our model is derived. By contrast the other proposals amount to adding up a series of locally driven flows, which may have some negative features. For example, *Griewank and Notz* [2013] might produce a relatively weak desalination of lower regions of ice, since in their parameterization the brine flux (implicitly vertical velocity) would not strictly increase with z there. Likewise, the decision to moderate the velocity in terms of a local Rayleigh number in *Turner et al.* [2013] might also produce a relatively weak desalination of the lower regions of the ice, since the local Rayleigh number approaches zero at the ice–ocean interface. In *Turner et al.* [2013], the fact that w is allowed to be non-zero at $z = 0$ might lead to relatively strong desalination near the top of the ice.

Furthermore, our model is a single description of gravity drainage derived from the physical CAP model, and avoids relying on other mathematical descriptions that are less obviously physically motivated, such as the 'simple model' used as a computationally cheap, stand-alone parameterization in *Griewank and Notz* [2013] and the 'slow mode of gravity drainage' used as an additional part of the parameterization in *Turner et al.* [2013]. These extend (in significantly different ways) the simple relaxation scheme for gravity drainage of *Vancoppenolle et al.* [2009a].

2.4. Boundary conditions at the ice–ocean interface

We assume that the temperature of the interface is equal to the liquidus temperature at the salinity of the well mixed ocean [*Worster*, 1986] and that the bulk salinity is continuous, which is equivalent to a zero solid fraction at the interface, consistent with the field observations of *Notz and Worster* [2008]. Therefore,

$$T = T_L(C_l), \quad S = C_l \qquad (z = h). \tag{14}$$

The growth of sea ice is determined by conservation of heat at the interface. A balance of heat fluxes across a control volume enclosing the interface and thin thermal boundary layer in the ocean gives

$$c_l \left[T_l - T_L(C_l)\right] \left(\dot{h} - w\,|_{z=h}\right) + L\dot{h}\phi\,|_{z=h} + F_T = k_m \frac{\partial T}{\partial z}\bigg|_{z=h}. \tag{15}$$

The first term is the advective heat flux across the thin thermal boundary layer [*Kerr et al.*, 1990], which is often small.

In laboratory experiments, the turbulent heat flux from the ocean F_T is caused by natural convection driven by the density difference $\Delta\rho$ between fluid at the interface and fluid in the interior, in which case

$$F_T = \left(2^{4/3}\lambda\right) k_l \left(\frac{\alpha_T g c_l}{k_l \nu}\right)^{1/3} \left[T_l - T_L(C_l)\right]^{4/3}, \tag{16}$$

where $\alpha_T = \alpha_T\left(T_L\left(C_l\right), C_l\right)$ is a temperature and salinity-dependent thermal expansion coefficient calculated from the density measurements of *Ruddick and Shirtcliffe* [1979]. The ocean is cooled by the turbulent heat flux and evolves according to

$$c_l (H - h) \frac{dT_l}{dt} = -F_T. \tag{17}$$

For implementation in a climate model, a friction velocity could alternatively be used in calculating F_T [*Maykut and McPhee*, 1995]. Indeed, the ice thickness after sufficiently long times is known to be very sensitive to the parameterization of oceanic heat flux [*e.g. Maykut and Untersteiner*, 1971; *Holland et al.*, 1997], and weaknesses in our parameterization of F_T may explain some of the discrepancy between our model and experimental observations shown in section 3.3. Note that, in our model, the term for latent heat released at the interface in equation (15) $L\dot{h}\phi\,|_{z=h} = 0$, since the solid fraction there is zero. However, we retain it to accommodate fixed-salinity models, in which the solid fraction at the interface is nonzero, for comparison in section 4. In this, we differ significantly from *Turner et al.* [2013] in that they treat the solid fraction at the interface as a tuning parameter that they adjust to match ice-thickness data.

The salt flux from the sea ice to the ocean

$$F_S = -\int_0^h \frac{\partial S}{\partial t}\, dz + \dot{h}\Delta S \tag{18}$$

is caused by the net change in the internal salinity of the ice and brine rejection at the ice–ocean interface associated with

a salinity discontinuity ΔS there. In our model, $\Delta S = 0$ (from equation 14) and the change to internal bulk salinity is caused by gravity drainage alone.

As ice grows, the salinity of the remaining well mixed ocean increases according to

$$(H - h)\frac{dC_l}{dt} = F_S. \tag{19}$$

However, within our numerical scheme, we prefer to apply global conservation explicitly by integrating the bulk salinity of the sea ice numerically. Further details about our numerical method are given in appendix B and *Rees Jones* [2014].

2.5. Model calculations

In order to illustrate the general behaviour of our model, figure 3 shows our results for a simulation in which ice is grown from a cold plate at constant temperature $T_B = -20°\mathrm{C}$. For this calculation, we fixed the salinity $C_l = 35.5$ ppt and temperature $T_l = -1.9°\mathrm{C}$ of the ocean to simulate a constant ocean heat flux of 29 $\mathrm{W/m^2}$, higher than average for the central Arctic Ocean [*Maykut and Untersteiner*, 1971]. As the sea ice grows, we continually update the temperature and salinity fields within the ice and use these to calculate the solid fraction (equation 2) and local Rayleigh number (equation 10) used in our parameterization of convection.

The temperature field (figure 3*a*) is approximately linear with depth, so the sea ice grows approximately diffusively (with the square root of time) with a balance between internal latent heat release and conduction to the cold plate. At later times the temperature gradient reduces, so the heat flux from the ocean becomes significant and slows the ice growth, eventually leading to a steady state. In these respects, our model differs little from other thermodynamic sea-ice models.

However, by allowing the salinity field (figure 3*b*) to evolve, our model captures the gradual desalination of sea ice caused by convection, which leads to C-shaped salinity profiles similar to those commonly observed in first-year ice. The elevated near-surface salinities in our model arise because $w = 0$ at $z = 0$ in equation (5), in contrast to *Turner et al.* [2013], which might explain their difficulty in obtaining C-shaped profiles. Throughout the calculation, the salinity at the interface with the ocean region remains constant. The amount of desalination is controlled by the choice of critical Rayleigh number R_c: at smaller R_c, the ice desalinates more before convection shuts down. We explore this effect more thoroughly in section 3, in which we compare predicted salt fluxes against those observed in laboratory experiments. At the ice–cold-plate interface, the salinity is steady, since the vertical upwelling velocity associated with convective desalination is zero there.

The desalination of the sea ice causes the local solid fraction to increase over the course of the experiment (figure 3*c*). Note that the rapid change in solid fraction near the ice–ocean region interface causes a rapid change in thermal properties of the ice, causing some nonlinearity in the temperature field (which is sometimes more pronounced than in figure 3*a*).

The local Rayleigh number (figure 3*d*) typically peaks around the chosen R_c because desalination causes the local Rayleigh number to relax back towards this value. There is usually one peak near the ice–ocean interface, and another near the cold plate. We suspect the latter is a result of our neglect of solar radiation, and brine expulsion, which would transport salt downwards within the ice, increasing the solid fraction in the upper ice and thereby reducing the permeability and local Rayleigh number. We discuss its evolution further when discussing convection in laboratory experiments (section 3.2.2).

3. Results in comparison with laboratory experiments

3.1. Discussion of experimental systems

We test our parameterization of gravity drainage by comparing its predictions to the results of two sets of laboratory experiments reported in *Wettlaufer et al.* [1997] and *Notz* [2005]. The latter is reported in less detail in *Notz et al.* [2005] and *Notz and Worster* [2008]. The basic systems are very similar: a coolant is circulated to maintain at constant temperature a brass cold plate mounted at the top of an insulated tank of horizontal size 20×20 cm and vertical size 37.6 cm for *Wettlaufer et al.* [1997] and 39.5 cm for *Notz* [2005]. Temperature is measured with thermistors, and salinity by measuring with an optical refractometer small samples withdrawn from the tank using a hypodermic syringe. The resolution of the refractometer used to measure salinity is approximately 1 ppt so measurements near the onset of convection (when salinity begins to rise from the initial value) are difficult. We also mention more briefly the older experiments of *Cox and Weeks* [1975], which differ more significantly from the other two sets. The most significant difference for our purposes is the size and shape of the tank, which is cylindrical, 14 cm in diameter and 69 cm deep.

To make a fair comparison with our model, it is important to be aware of experimental uncertainties. It is well known that heat fluxes from the laboratory affect ice growth and need to be minimized. In *Wettlaufer et al.* [1997] the insulated tank was placed in a larger environment, held at roughly 4°C. In *Notz* [2005], the tank was placed inside a freezer whose temperature was controlled to lie between 0°C and −1.5°C. The other significant difference is that in *Notz* [2005] a wire harp was fixed inside the tank to measure the electrical impedance between pairs of wires to determine the local solid fraction, while in *Wettlaufer et al.* [1997], measurements of volume expansion were used to determine the average solid fraction in the sea ice. The wire harp may affect brine drainage. Other differences are either unspecified or thought to be minor, at least at moderate to late times.

To some extent we privilege the experiments of *Wettlaufer et al.* [1997], not because they are necessarily better, but because they were conducted across a wider range of experimental conditions, which gives a more thorough test of our parameterization of gravity drainage.

Our approach complements the focus of *Turner et al.* [2013] and *Griewank and Notz* [2013] in that they each consider one laboratory experiment and one field experiment. Taken together with our study, they show the predictive capabilities of new parameterizations of gravity drainage. Whereas the previous two of these studies focus on salinity profiles take from the data of *Notz* [2005], we focus on measurements of the salinity of the ocean as a measure of the geophysically important salt flux from sea ice. *Griewank and Notz* [2013] acknowledge that the profiles they use have a typical uncertainty of around 5 ppt, and our independent analysis of the same experimental data suggests that they systematically underestimate the salinity of the ice. By comparison, we estimate that the uncertainty in the ocean salinities corresponds to an uncertainty of around 2 ppt in average ice salinity at the end of the experiment based on conserving salt within the experimental system, but with a bias towards overestimation caused by very salty water ponding at the bottom of the tank. For example, *Notz* [2005] observed a difference between measurements of salinity at the bottom and middle of the tank (figure 4) that may indicate accumulation, as well as some experimental scatter. By contrast,

measurements of thickness are somewhat more repeatable. If the average ice salinity is calculated without accounting for the mass of salt contained in liquid that overflows due to the lower density of ice (data for the overflow is not always available to us, so we do not use it in our calculations), there is a further overestimation of ice salinity by around 2–3 ppt in our treatment of the experimental data.

There are inconsistencies between experiments carried out at nominally equivalent conditions. Our comparison (figure 4*a*) between the experiments suggests that the thickness of sea ice observed by *Wettlaufer et al.* [1997] is less (by up to 15%) than that observed by *Notz* [2005] and *Cox and Weeks* [1975]. There is also almost certainly some differences in ocean salinity (figure 4*b*), since the different depths of the tank do not explain all the discrepancies between measurements. The experimental inconsistencies and biases in processing data must be remembered when comparing our models and choice of tuning parameters. These uncertainties should be addressed in future experiments.

3.2. Typical results for a fixed cold-plate temperature

We consider a constant cold-plate temperature of $T_B = -20^\circ$C and initial salinity 35.5 ppt, and compare our model results to the experimental observations of *Wettlaufer et al.* [1997]. The relatively low temperature of the cold plate means that heat gains from the laboratory are somewhat less important than for higher temperatures.

3.2.1. Time evolution

We show results for a range of tuning parameters and discuss sensitivity to them below. In figure 5*a* we show that our model predicts the approximately diffusive growth of sea ice over time reasonably well. Our model also reproduces the evolution of the ocean salinity well (figure 5*b*) for parameters around $R_c = 40$, $\alpha = 0.03$. (This choice is not particularly well constrained by the experiments and we return to this issue below.) However, it predicts a time for the onset of convection that is somewhat too early.

The temperature of the ocean (figure 5*c*) has been difficult to model across all the experiments. This discrepancy may arise owing to problems in our model, such as the assumption that the ocean is well-mixed, or experimental problems such as heat gains from the laboratory. The latter is suggested by the fact that the amount of superheat $T_l - T_L(C_l)$ increases after the first 10 hours, while our model predicts that it remains roughly steady.

3.2.2. Parameterization of convection and sensitivity to tuning parameters

In our parameterization of convection, a smaller value of R_c (which corresponds to a smaller critical thickness of ice for convection) means that convection begins earlier (figure 5*b*). However, R_c also determines the late-time evolution of the salinity field. A smaller R_c means that the ice can desalinate more (corresponding to a higher solid fraction and a smaller permeability) before convection shuts down, leading to a more saline ocean.

The sea-ice thickness predicted by our model without convection is consistently greater than that measured in experiments (figure 5*a*). All the parameterizations that include convection do a better job of describing the thickness, and can do so within the range of experimental uncertainty. However, the thickness appears relatively insensitive to the value of R_c because, although the thermal properties of ice depend significantly on salinity, the reduced thermal conductivity of more saline ice is almost balanced by the lower latent heat release. The trend towards slightly thicker ice when R_c is larger is consistent with the fact that more saline ice is slightly thicker, as discussed in section 4.3.

More systematically, in figure 6 we consider how the predicted salinity of the ocean and sea-ice thickness after 30 hours (the end of the experiment) depend on the tuning parameters. Firstly, in figure 6*a*, the ocean salinity depends strongly on the choice of parameters. The experimental uncertainty in ocean salinity corresponds to a large uncertainty in the choice of tuning parameters, and a significant area of parameter space is consistent with the single measurement of salinity at 30 hours. However, for there to be a significantly delayed onset of convection (at least a few hours), the critical Rayleigh number needs to exceed about 30. In this region of parameter space, the dependence on α is rather weak, so we fix $\alpha = 0.03$, a typical value in the idealized studies of *Rees Jones and Worster* [2013a]. There is some early-time sensitivity to α, but very little sensitivity several hours after the onset of convection because of the following negative feedback. A greater initial desalination increases the solid fraction, thereby reducing the Rayleigh number and so reducing later desalination. While we suggest using $R_c = 40$ for the *Wettlaufer et al.* [1997] experiments, a range $20 < R_c < 45$ would be reasonable. Were we prepared to relax the constraint that convection is delayed for a few hours (such a delay is much less clear in the experiments of *Notz* [2005], for example, shown in figure 4*b*, and may not be so important geophysically), a rather different choice of parameters would be possible (such as, say, $R_c = 5$, $\alpha = 0.003$ to give an illustrative example that we use later in figure 11). This is perhaps not unreasonable given that the CAP model is based on fully developed channels and so may not apply well immediately after the onset of convection. Incidentally, using measurements of salinity at different times (sufficiently long after the onset of convection) and different experiments provides only a weak constraint on the choice of parameters since, for example, this alternative choice of parameters would also produce reasonable results in figure 8 given the experimental uncertainty. Secondly, in figure 6*b*, the sea-ice thickness depends only weakly on the choice of parameters. Therefore, observations of thickness are not a suitable way to constrain the parameterization.

Our parameterization predicts that convection is confined to a lower layer of ice for much of the time. The detailed behaviour is sensitive to the precise details of the parameterization – using the approach described in section 2.3 leads to cycles of full-depth and confined convection, at least for the early part of ice growth in a confined tank (figure 7) for sufficiently large α (note that, for example, $\alpha = 0.003$ would not exhibit this behaviour but full-depth convection would persist for much longer). The basic mechanism driving these cycles is as follows: a shift to confined convection reduces the salt flux from the ice, leading to a slower increase in solid fraction and slower decrease in permeability. However, the growth rate is almost unchanged, so the local Rayleigh number can increase sufficiently to allow full-depth convection. The more rapid desalination then decreases the permeability faster, leading to convection being confined again. This behaviour is quite common in our model and indeed the signature of these oscillations is shown in the Ra-profiles shown in figure 3*d* for a deep tank with the Rayleigh number at the top of the tank $Ra(0)$ switching between being just supercritical and just subcritical. This switching allows the upper regions of ice to desalinate slowly (*cf.* figure 3*c*) within our single parameterization of gravity drainage, which may have a similar effect to the additional 'slow mode of gravity drainage' that *Turner et al.* [2013] introduce. We note in passing that oscillations in gravity drainage have previously been reported in experiments; for instance *Eide and Martin* [1975] report oscillations with a period of roughly an hour in 10 cm-thick ice.

3.3. Predictions of 1D model with fixed chill

The usefulness of our model does not depend on its ability to predict a single experiment. Arguably, it is not surprising that any reasonable model could achieve this by adjusting

tuning parameters. Therefore, we run our model with the same tuning parameters $R_c = 40$, $\alpha = 0.03$ suggested by the cold-plate temperature $T_B = -20^\circ$C over a range of fixed $T_B = -10, -15, -20^\circ$C. There is a tendency to overestimate sea-ice thickness in our model, which occurs to greater extent at warmer T_B (figure 8*a*). This seems likely to result from heat gains from the laboratory discussed in section 3.1.

In terms of ocean salinity, the onset of convection is not particularly well described by our model. According to our model, the onset is earliest in the case $T_B = -10^\circ$C, which is the reverse of the experimental observations (figure 8*b*). Given that predictions of sea-ice thickness for early times are reasonably accurate, this discrepancy is most likely to be connected to difficulties in calculating the permeability of mushy layers. There appears to be a systematic tendency to overestimate the permeability of relatively porous ice ($T_B = -10^\circ$C) but underestimate the permeability of less porous ice ($T_B = -20^\circ$C). We return to this question in section 5. Nevertheless, our model describes the evolution of both the sea-ice thickness and salinity of the ocean across all three experiments in a reasonably successful fashion.

3.4. Predictions of 1D model with variable chill

We compare our model to an experiment by *Notz* [2005] in which the cold plate temperature was switched every twelve hours, a timescale chosen to mimic a diurnal cycle. We use tuning parameters $R_c = 20$, $\alpha = 0.03$ suggested by the equivalent experiment at fixed cold-plate temperature (*cf.* figure 4, but note that the different R_c is associated with the experimental inconsistency discussed in section 3.1). Our model does a very good job of reproducing the observed sea-ice thickness and desalination of the ice (figure 9). Although these step changes in temperature are somewhat artificial, very similar results were obtained in our model with a sinusoidally varying cold-plate temperature.

3.5. Discussion

Calculations of sea-ice thickness are sensitive to knowledge of the thermal properties of ice. In our calculations, we have made a number of approximations, such as ignoring the variation in these properties with temperature. Nevertheless, we are able to predict ice growth within experimental uncertainty, albeit with a bias of over predicting growth. Crucially, a single (but perhaps not unique) choice of tuning parameters can successfully describe the evolution of the salinity of the ocean in a range of experiments at different conditions. Therefore, our parameterization represents promising progress in the accurate, time-dependent, prediction of salt fluxes in sea-ice models.

However, there are differences between experiments (which we do not fully understand) and biases in processing experimental data that would lead to different (lower) choices of critical Rayleigh number compared to those based on the measured ocean salinity in the experiments of *Wettlaufer et al.* [1997] on which we have focused. Taking into account both the measurement uncertainty and processing bias discussed in section 3.1, we estimate that the average ice salinity implied by conservation of salt within the experimental system could be as much as 5 ppt too high. This crucial consideration must be remembered when we consider the implications for climate models in the next section. Furthermore, if we did not insist that convection was delayed for several hours, a very different choice of tuning parameters (with much lower α and R_c) is possible. The salinity to which the sea ice desalinates is very sensitive to R_c, so a possible approach is to constrain R_c using very late time observations (from much longer experiments) and then use the comparatively early experiments (for example the experimental curve in figure 6*b*) to determine α. Thus further experiments are required to resolve the final choice of parameters.

4. Implications for climate models: comparison with a fixed-salinity model

Having developed a functioning dynamic-salinity sea-ice model, we assess the implications for climate models by comparing it with a fixed-salinity model. We use version 4 of CICE: The Los Alamos Sea Ice Model [*Hunke and Lipscomb*, 2008] (henceforth referred to as 'CICE') for parameter values of such a model, but note that the more recent version 5 incorporates as an option the parameterization of *Turner et al.* [2013]. It is important to note that CICE was not designed to simulate small-scale experiments in which the ice is relatively salty but rather for longer periods when the ice is more desalinated as a result of not only gravity drainage, but also other processes that affect ice salinity (section 1.2). Nevertheless the comparison is instructive because it shows the consequences of using a fixed-salinity model.

The thermodynamic modeling in *Bitz and Lipscomb* [1999], incorporated into CICE, is approximately equivalent to that derived from mushy-layer theory. In particular, *Feltham et al.* [2006] show that if the liquidus relationship is taken to be linear $C_L(T) = -T/\Gamma$, then equations (6, 9) for the thermal properties of a mushy layer simplify to

$$c_i(T,S) = c_s + L\Gamma\frac{S}{T^2}, \tag{20}$$

$$k_i(T,S) = k_s + \Gamma\left(k_s - k_l\right)\frac{S}{T}, \tag{21}$$

which are exactly the same expressions used in CICE, except for the small difference that $\Gamma\left(k_s - k_l\right)$ is replaced by a constant 0.0013 W/cm/ppt. In the case of CICE, k_i artificially drops to zero at the ice–ocean interface where the temperature $T_O \approx -2^\circ$C when the bulk salinity $S = k_s(-T_O)/0.0013 \approx 33$ ppt. By contrast, in our calculations k_i is always greater than the thermal conductivity of brine and so never drops to zero. In our comparisons, we use equations (20) and (21) with the constant 0.0013 W/cm/ppt as mentioned above and parameter values taken from the CICE documentation for consistency. The most significant difference is that the default option for the thermal conductivity of pure ice is 0.0203 W/cm/deg, which is lower than most estimates, including that used in table 1 [*cf. Pringle et al.*, 2007] – which has the effect of reducing ice growth slightly.

In this section, we perform a series of calculations (using various boundary conditions) of the thermodynamic growth of sea ice, in which the thermal properties are calculated either as in CICE (described immediately above), or using our full dynamic-salinity calculation (described in section 2). In all other respects (numerical method, treatment of the ocean, including the relationship between its salinity and melting temperature), our models are the same. This isolates the importance of the salinity of sea ice for its thermodynamic growth.

4.1. Comparison with CICE for laboratory experiments

The default CICE option (CICE–def) is to use a fixed-salinity profile $S_i(\zeta) = 0.5 \times 3.2\left[1 - \cos\left(\pi\zeta^{0.407/(\zeta+0.573)}\right)\right]$, where $\zeta = z/h$, for thermodynamic growth, and a constant reference salinity $S_i = 4$ ppt for ice–ocean salt exchange. We later consider the effect of using uniform salinities $S_i = 4$ ppt (CICE–4) and $S_i = 25$ ppt (CICE–25) for both thermodynamic and ice–ocean salt exchange calculations. $S_i = 25$ ppt is the average ice–salinity after 30 hours in the experiment of figure 10.

For a fixed cold-plate temperature, all the models do a reasonable job of predicting sea-ice thickness (figure 10*a*), but this is because growth depends only weakly on salinity (section 4.3.1), with a progressively worse agreement for low ice salinity. We show below (section 4.3.2) that CICE is principally sensitive to salinity through changes to the ocean salinity, so much of this discrepancy is explained by the very large over prediction of ocean salinity (figure 10*b*). This is a proxy for salt fluxes to the ocean, so the over prediction of ocean salinity in the CICE calculations corresponds to an over prediction of the initial salt flux, which arises from excessively high brine rejection at the ice–ocean interface. Although it is possible to choose a value of the ice salinity S_i to match an experimental result of ocean salinity at a given time, CICE predictions are fundamentally inconsistent with the time evolution of the salinity. Note that the CICE–def and CICE–4 profiles give indistinguishable predictions. This suggests that using depth-dependent salinity profiles does not affect the initial growth of sea ice, although for late times the salinity at the interfaces matters. We also tested the variable-cold-plate-temperature scenario of section 3.4, which had a similar pattern of discrepancies, but slightly greater, suggesting that our dynamic-salinity model copes better with varying heat fluxes (*cf.* figure 15*b*).

In conclusion, the differences in predictions of sea-ice thickness are relatively small and have a similar magnitude to the uncertainties in experiments and material properties. However, the differences in predictions of salt fluxes are large and systematic. Therefore, the greater success of our dynamic-salinity model strongly suggests that it would improve the representation of salt fluxes into the polar oceans.

4.2. Comparison with CICE for a deep ocean

Results for solidification into a deep ocean are arguably more important than into a tank. However, lacking sufficient experimental data to assess which model is superior, in this section we show that our dynamic-salinity model gives substantially different predictions of ice growth and discuss possible implications for climate models.

To compare models, we assume the ocean is very deep and hence that its temperature $T_l = -1.9^\circ\mathrm{C}$ and salinity $C_l = 35.5$ ppt are constant. These conditions impose a constant ocean heat flux of 29 $\mathrm{W/m^2}$. Thus we explicitly neglect changes to the salinity of ocean (which would otherwise cause further differences between models in terms ice growth). A more detailed ocean model is needed to assess these feedbacks properly.

Initially our dynamic-salinity model predicts greater growth than in CICE, as shown in figure 11*a* (inset). This is exactly as we found in our tank experiments. The variation with ice salinity observed is caused by the change in physical properties (*cf.* section 4.3.1).

However, after longer periods (several weeks), this trend is reversed and the CICE model predicts greater growth than our dynamic-salinity model. At late times, growth depends dominantly on the thermal conductivity near the ice–ocean interface (*cf.* section 4.3.3). In our dynamic model, this is always equal to the conductivity of the liquid phase (since $\phi = 0$ at the interface, independent of the mean ice salinity) whereas in a fixed-salinity model (in which $\phi > 0$ at the interface) the conductivity will always be higher. Therefore, our model's continuous bulk salinity profile at the ice–ocean interface makes a measurable difference to predictions. In practice, the effect of thermal conductivity would need to be considered alongside the effect of high-frequency forcing and snow cover.

The difference in ice thickness is in addition to the difference between the models in average ice salinity (figure 11*b*), which is a measure of the total salt flux into the ocean. Note that the predicted sea-ice salinities in our model are rather high for first-year ice [*Weeks*, 2010] using the high choice $R_c = 40$ suggested by the experiments of [*Wettlaufer et al.*, 1997], which is partly a consequence of our constant atmospheric temperature. Periods of warming (and the absorption of shortwave radiation later in the Spring and Summer) would result in a lower solid fraction and hence a more permeable mushy layer that could desalinate further, as was observed in the simulations of *Turner et al.* [2013] and *Griewank and Notz* [2013] with realistic forcing. We also include calculations with an alternative choice of parameters $R_c = 5$, $\alpha = 0.003$. These parameters are also consistent with the late-time aspects of laboratory experiments (see section 3.2.2 and figure 6). With such parameters, the ice desalinates considerably more, and so similar alternative choices could potentially be more appropriate for climate models.

4.3. Discussion: physical mechanisms by which salinity affects ice growth

In this section we present simplified calculations of thermodynamic growth using the CICE-type fixed salinity model introduced previously. We use a constant, uniform ice salinity S_i in both the thermodynamic and ice–ocean salt exchange calculation. We separate the effects of variation in the thermodynamic properties with S_i and changes to the environment over time that also depend on S_i indirectly through salt fluxes.

4.3.1. Effect of the thermodynamic properties of ice

More saline ice has a lower solid fraction and so has a lower thermal conductivity. However, there is also less latent heat of solidification, which counterbalances the decrease in conductivity. We analyze this balance systematically by considering an infinitely deep tank and neglecting any heat flux from the tank.

In the solid $t = 0$ curve in figure 12*a*, we show that the average growth rate, measured in $\mathrm{cm^2/hour}$ to reflect the fact that the growth of ice is exactly diffusive in this scenario, depends only very weakly on the prescribed salinity of the ice. By 'exact diffusive growth' we mean that the sea-ice thickness is proportional to the square root of the time for which it has been growing. Indeed, this scenario can be analyzed asymptotically (we intend to publish details at a later date) and this asymptotic analysis shows that this graph is representative of a wide class of similar situations in which the thermal properties of a material vary with salinity. In particular, the weak increase in growth rate with increasing salinity is generic across the entire range of T_B relevant to sea-ice formation. Therefore, vertical salinity variation is not particularly important for the growth rate of first-year ice. Our analysis constitutes a general explanation of this effect noticed for first-year ice by *Vancoppenolle et al.* [2005] and observed by *Griewank and Notz* [2013] in their calculations.

4.3.2. Effect of changing ocean salinity over time

In a finite tank, using a lower ice salinity for the ice–ocean salt exchange means that the ocean becomes more saline over time because there is more segregation at the interface. This depresses the freezing temperature of the ocean $T_L\,(C_l)$, which is the temperature of the ice–ocean interface, and thereby reduces the temperature difference across the sea ice. The reduction decreases the conduction of heat across the ice and causes slowing growth rates over time as shown in figure 12*a*. Thus the dependence on ice salinity caused by changes to the physical properties of ice is still present, but at later times that effect is dominated by changes to the ocean salinity.

4.3.3. Effect of prescribed heat flux from the ocean

We prescribe a fixed heat flux and salinity of the ocean. The situation here is more complex: at early times, the results of section 4.3.1 apply, but at late times the heat flux from the ocean will always be significant and balanced by

the conductive heat flux from the relatively warm ocean. This balance gives a steady-state thickness

$$h \sim k_i(z = h)\Delta T/F_T. \quad (22)$$

Although a steady state is certainly not achieved in (say) 30 days of growth, the balance of fluxes represented by equation (22) is nevertheless important over this timescale. Therefore, the dependence of the thermal conductivity near the ice–ocean interface on salinity determines the growth rate: k_i decreases with S_i (equation 21, reflecting the fact that more saline ice has a lower solid fraction) so h decreases with S_i. Since the steady-state thickness is lower for higher S_i, the average growth rate at sufficiently late times must also be lower, as shown in figure 12*b*. The trend is only enhanced at later times (figure 11). Note that this effect was reported in terms of the bottom growth by *Vancoppenolle et al.* [2005] for multi-year ice at a few values of S_i; however, in their calculations the effect was more than counteracted by changes in surface melting, which we do not consider in our test calculations. This suggests that our dynamic-salinity model will cause additional differences when the ice starts to melt in the summer.

5. Relationship between the porosity and permeability of sea ice

Calculations of local Rayleigh number in our model (and in other similar models) use a permeability that depends on the porosity of the ice. The relationship between the porosity and permeability of a reactive porous medium, such as sea ice, is an intrinsically difficult problem because direct measurements alter the structure of the medium. Some recent progress, reviewed by *Golden et al.* [2007], has been made by taking essentially microstructural models that have some form of *local* permeability and using them to establish a *bulk* permeability for a layer of sea ice [*e.g. Petrich et al.*, 2006; *Zhu et al.*, 2006].

Our dynamic-salinity model of sea ice applies to a much wider class of problems than simply those growing sea ice from saltwater with a salinity of about 35 ppt, because it is derived from fundamental physics and was not particularly designed for sea ice (with the exception of the tuning parameters R_c and α, which we do not use in this section because here we only consider behaviour before the onset of convection). Thus we have used it to investigate the full set of experiments considered in *Wettlaufer et al.* [1997], which were conducted at different initial saltwater salinities from 20 to 140 ppt. These lead to the formation of ice with different porosities, allowing an indirect study of the relationship between porosity and permeability.

Here, we extend a suggestion of *Wettlaufer et al.* [1997, 2000]: the hypothesis of a constant critical Rayleigh number can be used to collapse data from the full range of experiments to a single curve and this curve used to infer the (bulk) permeability. We extend this suggestion by inferring a consistent local permeability.

Our procedure is as follows. We take the experimental measurements in *Wettlaufer et al.* [1997] of ocean salinity as a function of sea-ice thickness and use them to calculate a critical thickness for the onset of convection (at which the ocean salinity starts to increase from its initial value). We then use our model, forced at the relevant experimental conditions, to calculate the growth of the mushy layer until the experimental critical thickness is reached. We calculate the local Rayleigh number from equation (10) at the critical thickness assuming a given relationship for the local permeability $K_l(\phi) = (1-\phi)^b$ in equation (11). We then plot the maximum value of the Rayleigh number $Ra_{\max}$ against the calculated mean solid fraction $\overline{\phi}$. We look for a horizontal line of best fit, because a constant $Ra_{\max}$ with $\overline{\phi}$ corresponds to the hypothesis of a constant critical Rayleigh number.

In figure 13*a*, we show that local permeability $K_l(\phi) = (1-\phi)^3$ does not appear consistent with a constant critical Rayleigh number. The cubic relationship seems to overestimate the permeability for low solid fraction and underestimate it for high solid fraction, consistent with the pattern observed in figure 8 and also the measurements of *Eicken et al.* [2004]. A better choice, shown in figure 13*b*, is $K_l(\phi) = (1-\phi)^2$, which successfully removes most of the trend evident in figure 13*a* and is consistent with the hypothesis of a constant critical Rayleigh number. It also corrects the problems with predicting onset noted in figure 8*b* and improves predictions throughout the range of times considered.

It is important to note that, in the interpretation of experiments in figure 14, the hypothesis of a constant critical bulk Rayleigh number is nevertheless consistent with a bulk permeability that varies cubically with mean porosity, *i.e.* $\overline{K} \propto (1-\overline{\phi})^3$, a relationship commonly suggested following *Freitag* [1999]. This suggests that caution should be used when calculating a local Rayleigh number using formulae appropriate to the bulk permeability. A local permeability $K_l(\phi) = (1-\phi)^2$ corresponds to a microstructural model of cylindrical tubes orientated parallel to the temperature gradient [*e.g. Phillips*, 1991], which is plausible for sea ice. Coupled with the promising results from our model, this leads us to propose investigating this relationship in future when calculating local Rayleigh numbers.

6. Conclusions

Our new dynamic-salinity sea-ice model contains a parameterization of gravity drainage derived from fundamental physical principles governing convection in a porous medium. Thus it can account for important dynamical feedbacks that regulate the desalination of sea ice, such as the relationship between ice salinity, porosity, permeability and the desalination rate (which we use a local Rayleigh number to represent), as well as varying external forcing from the atmosphere and ocean. It incorporates the same physics governing both the delayed onset of convection, and also its subsequent confinement, which is certainly relevant on geophysical timescales. Thus it could account for temporary intermittent salt fluxes to the ocean associated with, for example, the sudden warming of sea ice.

Our simple parameterization benefits from being a single governing equation for the vertical transport of heat and salt caused by convection. We have expressed our parameterization in terms of the underlying partial differential equations, rather than a particular numerical scheme, such that it can be implemented readily in climate models using any desired numerical method. In general, the numerical cost of using our parameterization should be comparable to, for example, *Turner et al.* [2013], since our parameterization is essentially a different way of calculating the advective transport term due to gravity drainage. Our treatment of the thermodynamics of sea-ice growth is based on mushy-layer theory, accounting for a nonlinear liquidus relationship, and is consistent with current sea-ice models. Our model can be solved with a variety of boundary conditions; in particular, the atmospheric and ocean heat fluxes ocean could be imposed. Thus our model could be incorporated into a fully coupled climate model, with other desalination mechanisms also represented to model growth over many seasons.

As well as being physically based (in common with some of the other new generation of dynamic-salinity sea-ice models), our model has been thoroughly tested against a wide range of published laboratory experiments. We have successfully used a single choice of tuning parameters to predict

the salt fluxes across a range of experimentally imposed external conditions. There are significant inconsistencies and biases between experiments at nominally the same conditions, which leads to some uncertainty in the final choice of tuning parameters. In particular, if experiments were designed to particularly measure the average ice salinity as a function of time over a longer period, or if the experimentally observed delay in the onset of convection were not used to partly constrain the choice of parameters, rather different parameters could be chosen with much smaller values of critical Rayleigh number and proportionality factor. This would lead to more desalinated ice in deep-ocean calculations, and therefore may be more appropriate for climate models. Further laboratory experiments (and perhaps field observations) are needed to resolve this choice.

Finally, we have shown that our dynamic parameterization of ice salinity causes some differences from established, fixed-salinity models in terms of predicted ice thickness and much more significant differences in terms of the qualitative pattern and quantitative magnitude of salt fluxes (shown in figure 15). Prescribing a low ice salinity when calculating ice–ocean salt exchange in climate models is equivalent to predicting an excessive salt flux due to segregation at the interface and is inappropriate for thinner, first-year ice. Thus accounting for salt transport reduces salt fluxes, consistent with the pattern found in previous studies [*e.g. Vancoppenolle et al.*, 2009b]. We have presented the different predictions in a number of ideal, representative scenarios. The physical basis and success of our model in predicting laboratory experiments gives us reason to expect that it should be more successful in predicting salt fluxes in climate models. Therefore, we expect that our parameterization should improve the predictive capabilities of sea-ice models, making them more robust to climate change and more responsive to short-term variability in external forcing.

Appendix A: Effective heat capacities

We derive expressions for the effective heat capacities of sea ice and brine transport, generalizing *Feltham et al.* [2006] to a nonlinear liquidus and giving a fuller derivation. A phase-averaged heat equation for a two phase porous medium is

$$[c_s\phi + c_l(1-\phi)]\frac{\partial T}{\partial t} + c_l w\frac{\partial T}{\partial z} = \frac{\partial}{\partial z}\left(k_i\frac{\partial T}{\partial z}\right) + L\frac{\partial \phi}{\partial t}. \quad \text{(A1)}$$

We use the expression for solid fraction in terms of bulk and interstitial salinity $1-\phi = S/C_L$ (equation 2) to determine the final term in equation (A1), which represents latent heat release. In particular, taking the derivative with respect to time, we find

$$-\frac{\partial \phi}{\partial t} = \frac{1}{C_L}\frac{\partial S}{\partial t} - \frac{S}{C_L^2}\frac{\partial C_L}{\partial t}, \quad \text{(A2)}$$

$$= -w\frac{C_L'}{C_L}\frac{\partial T}{\partial z} - \frac{SC_L'}{C_L^2}\frac{\partial T}{\partial t}, \quad \text{(A3)}$$

where we use salt conservation (4) to determine $\partial S/\partial t$ and the chain rule for derivatives. Substituting into equation (A1) and rearranging, we find

$$\left[c_s - (c_s - c_l)\frac{S}{C_L} - \frac{LSC_L'}{C_L^2}\right]\frac{\partial T}{\partial t} + \left[c_l - \frac{C_L'}{C_L}\right]w\frac{\partial T}{\partial z} = \frac{\partial}{\partial z}\left(k_i\frac{\partial T}{\partial z}\right). \quad \text{(A4)}$$

The first square bracket gives the required effective heat capacity of sea ice (equation 6) and the second for brine transport (equation 7). Note that in equation (6), we neglect the small term involving $(c_s - c_l)$ as discussed in section 2.2. Note also that $C_L' < 0$ so both these heat capacities are enhanced by latent heat release.

Appendix B: Solution method and initialization

A fuller description of our numerical method can be found in *Rees Jones* [2014]. We non-dimensionalize the governing equations and boundary conditions for numerical convenience. Sea ice occupies the region $0 \le z \le h(t)$. It is moderately difficult to accommodate a time-dependent domain numerically, although this is sometimes done in so-called 'enthalpy-methods' [*e.g. Oertling and Watts*, 2004; *Notz and Worster*, 2006], including, for example, version 4 of CICE [*Hunke and Lipscomb*, 2008]. In this paper, we map the sea ice to $[0, 1]$ by changing variables $\zeta = z/h$. This analytic mapping avoids the need to re-map a numerical grid, and the additional nonlinearity in the equations is not especially costly because the equations are already nonlinear. It has the computational advantage that the temperature is approximately steady in these changed coordinates. Rather than directly calculating $h(t)$, we calculate $h^2(t)$ to cope better with the initial growth.

If we set $w = 0$, our equations reduce to equivalent equations in *Kerr et al.* [1990]. Therefore, we use the same type of numerical method: a predictor-corrector generalization of the second-order in space Crank-Nicholson routine [*Ames*, 1977] solves the partial differential equations (3, 4), and a second-order Runge-Kutta routine solves the ordinary differential equations governing the interface location (15) and the temperature of the ocean (17). Our approach retains the stability advantages of semi-implicit schemes while retaining a linear tridiagonal system that can be readily solved.

In order to retain second-order spatial accuracy in extending this method to $w \neq 0$, we faced a number of challenges arising from our parameterization of convection. If the maximum Rayleigh number and critical depth was at the end point $z = 0$, there was no problem using a discrete grid. However, otherwise we fitted piecewise quadratic curves to each triplet of discrete values of the local Rayleigh number to maintain second-order spatial accuracy. Likewise, we used Simpson's rule when using quadrature to calculate the salt flux to the ocean. We explicitly conserved salt globally.

The numerical method was tested against known solutions for the linear and nonlinear heat equation without convection, and tested for resolution sensitivity. In all our calculations for the graphs in this paper we used 100 vertical grid points. However, our model can certainly be run with fewer grid points. For example, in calculations for figure 3, after 20 days of growth into a deep ocean the use of 40 grid points gives a difference of 0.7% in the change in average sea-ice salinity, 10 gives a difference of 5% in the change in average sea-ice salinity, and 5 gives a difference of 16% in the change in average sea-ice salinity. The differences between sea-ice thickness were small (at most about 2% after 20 days, although higher for earlier times). This suggests that it is practical to use our parameterization in climate models with 5 or 10 grid points, although it may be necessary to retune parameters for the smaller number of grid points. We did not use a fixed time step but instead controlled errors in time stepping by both imposing a Courant condition and also by calculating the difference between two time steps and a single time step of double the length. This gives an estimate of the error, which we used to adjust the time step such that the error remained below some specified tolerance. For example, in the calculation with 5 grid points discussed above, the average time step was about 30 minutes.

The initial conditions depend on the situation modeled and the following conditions are appropriate to the laboratory experiments in section 3. Initially the sea-ice thickness

is zero and, before convection begins, the bulk salinity of the ice has the same value as the initial salinity of the ocean so

$$h(0) = 0, \quad S(0,z) = C_0, \quad C_l(0) = C_0, \quad T_l(0) = T_0, \tag{B1}$$

where the initial salinity C_0 and temperature T_0 of the ocean must be specified.

While the initial temperature profile $T(0,z)$ appears arbitrary, it can be uniquely specified such that $h \sim At^{1/2}$ as $t \to 0$, for some constant A to be determined, which is exact diffusive growth. Exact diffusive growth corresponds to the initial temperature profile being steady in scaled coordinates ζ. Initially there is no convection, as observed by *Wettlaufer et al.* [1997] (the initial Rayleigh number will be zero, since the sea-ice thickness is zero). Then, asymptotically approximating the boundary condition (15) to determine the initial growth rate in terms of the initial temperature profile, the heat equation (3) becomes an ordinary differential equation, which we solve numerically using a shooting method and Runge-Kutta routine to uniquely determine the initial temperature profile.

Acknowledgments. We are grateful to John Wettlaufer and Dirk Notz for their experimental data, which are used in figures 4–6, 8–10 and 13–14. For further details, please see *Wettlaufer et al.* [1997], and *Notz* [2005]; *Notz et al.* [2005]; *Notz and Worster* [2008]. We would also like to thank Jerome Neufeld for helpful discussions and comments on an earlier draft of this paper, and M. Vancoppenolle and two anonymous referees.

References

Amberg, G., and G. M. Homsy (1993), Nonlinear analysis of buoyant convection in binary solidification with application to channel formation, *J. Fluid Mech.*, *252*, 79–98, doi:10.1017/S0022112093003672.

Ames, W. F. (1977), *Numerical Methods for Partial Differential Equations (2nd edn.)*, Academic.

Assur, A. (1958), Composition of sea ice and its tensile strength, in *Arctic sea ice*, pp. 106–138, U.S. Natl. Acad. Sci.

Aussillous, P., A. J. Sederman, L. F. Gladden, H. E. Huppert, and M. G. Worster (2006), Magnetic resonance imaging of structure and convection in solidifying mushy layers, *J. Fluid Mech.*, *552*, 99–125.

Batchelor, G. K. (1974), Transport properties of two-phase materials with random structure, *Ann. Rev. Fluid Mech.*, *6*(1), 227–255.

Bennington, K. O. (1963), Some crystal growth features of sea ice, *J. Glaciol.*, *4*(36), 669–688.

Bitz, C. M., and W. H. Lipscomb (1999), An energy-conserving thermodynamic model of sea ice, *J. Geophys. Res.*, *104*(C7), 15,669–15,677.

Chung, C. A., and M. G. Worster (2002), Steady-state chimneys in a mushy layer, *J. Fluid Mech.*, *455*, 387–411.

Cox, G. F. N., and W. F. Weeks (1975), Brine drainage and initial salt entrapment in sodium chloride ice, *CCREL Res. Rept.*, *345*.

Cox, G. F. N., and W. F. Weeks (1988), Numerical simulations of the profile properties of undeformed first-year sea ice during the growth season, *J. Geophys. Res.*, *93*(C10), 12,449–12,460.

Davaille, A., and C. Jaupart (1993), Transient high-Rayleigh-number thermal convection with large viscosity variations, *J. Fluid Mech.*, *253*, 141–166, doi:10.1017/S0022112093001740.

Eicken, H. (1992), Salinity profiles of Antarctic sea ice: Field data and model results, *J. Geophys. Res.*, *97*(C10), 15,545–15,557, doi:10.1029/92JC01588.

Eicken, H., T. C. Grenfell, D. K. Perovich, J. A. Richter-Menge, and K. Frey (2004), Hydraulic controls of summer Arctic pack ice albedo, *J. Geophys. Res.*, *109*(C08007), doi:10.1029/2003JC001989.

Eide, L. I., and S. Martin (1975), The formation of brine drainage features in young sea ice, *J. Glaciol.*, *14*, 137–154.

Feltham, D. L., N. Untersteiner, J. S. Wettlaufer, and M. G. Worster (2006), Sea ice is a mushy layer, *Geophys. Res. Lett.*, *33*(14), doi:10.1029/2006GL026290.

Freitag, J. (1999), Hydraulic properties of Arctic sea ice – implications for the small scale particle transport, *Rep. Polar Res.*, *325*.

Gent, P. R. (2012), Coupled climate and earth system models, in *Climate Change Modeling Methodology: Selected Entries from the Encyclopedia of Sustainability Science and Technology*, edited by P. J. Rasch, chap. 2, pp. 5–30, Springer New York, doi:10.1007/978-1-4614-5767-1_2.

Golden, K. M., H. Eicken, A. L. Heaton, J. Miner, D. J. Pringle, and J. Zhu (2007), Thermal evolution of permeability and microstructure in sea ice, *Geophys. Res. Lett.*, *34*(16), doi:10.1029/2007GL030447.

Griewank, P. J., and D. Notz (2013), Insights into brine dynamics and sea ice desalination from a 1-D model study of gravity drainage, *J. Geophys. Res.*, doi:10.1002/jgrc.20247.

Holland, M. M., J. A. Curry, and J. L. Schramm (1997), Modeling the thermodynamics of a sea ice thickness distribution: 2. Sea ice/ocean interactions, *J. Geophys. Res.*, *102*(C10), 23,093–23,107, doi:10.1029/97JC01296.

Hunke, E. C., and W. H. Lipscomb (2008), CICE: The Los Alamos sea ice model user's manual, version 4, *Los Alamos National Laboratory Tech. Rep.*, *LA-CC-06-012*.

Hunke, E. C., D. Notz, A. K. Turner, and M. Vancoppenolle (2011), The multiphase physics of sea ice: a review for model developers, *Cryosphere*, *5*(4), 989–1009.

Jardon, F. P., F. Vivier, M. Vancoppenolle, A. Lourenço, P. Bouruet-Aubertot, and Y. Cuypers (2013), Full-depth desalination of warm sea ice, *J. Geophys. Res.*, *118*(1), 435–447, doi:10.1029/2012JC007962.

Jeffery, N., E. C. Hunke, and S. M. Elliott (2011), Modeling the transport of passive tracers in sea ice, *J. Geophys. Res.*, *116*(C7), doi:10.1029/2010JC006527.

Kerr, R. C., A. W. Woods, M. G. Worster, and H. E. Huppert (1990), Solidification of an alloy cooled from above. Part 1. Equilibrium growth, *J. Fluid Mech.*, *216*, 323–342.

Lange, N. A., and G. M. Forke (1952), *Handbook of Chemistry*, 8th ed., Handbook Publ., Sandusky, Ohio.

Malmgren, F. (1927), On the properties of sea ice, in *The Norwegian North Polar Expedition with the 'Maud' 1918–1925*, vol. 1a, edited by H. U. Sverdrup, pp. 1–67, John Griegs Boktr., Bergen, Norway.

Maykut, G. A., and M. G. McPhee (1995), Solar heating of the Arctic mixed layer, *J. Geophys. Res.*, *100*(C12), 24,691–24,703, doi:10.1029/95JC02554.

Maykut, G. A., and N. Untersteiner (1971), Some results from a time-dependent thermodynamic model of sea ice, *J. Geophys. Res.*, *76*(6), 1550–1575.

Nakawo, M., and N. K. Sinha (1981), Growth rate and salinity profile of first-year sea ice in the High Arctic, *J. Glaciol.*, *27*, 315–330.

Notz, D. (2005), Thermodynamic and fluid-dynamical processes in sea ice, Ph.D. thesis, University of Cambridge, Cambridge, U. K.

Notz, D., and M. G. Worster (2006), A one-dimensional enthalpy model of sea ice, *Ann. Glaciol.*, *44*(1), 123–128.

Notz, D., and M. G. Worster (2008), In situ measurements of the evolution of young sea ice, *J. Geophys. Res.*, *113*(C3), doi:10.1029/2007JC004333.

Notz, D., and M. G. Worster (2009), Desalination processes of sea ice revisited, *J. Geophys. Res.*, *114*(C5), doi:10.1029/2008JC004885.

Notz, D., J. S. Wettlaufer, and M. G. Worster (2005), A non-destructive method for measuring the salinity and solid fraction of growing sea ice in situ, *J. Glaciol.*, *51*(172), 159–166, doi:doi:10.3189/172756505781829548.

Oertling, A. B., and R. G. Watts (2004), Growth of and brine drainage from NaCl–H_2O freezing: A simulation of young sea ice, *J. Geophys. Res.*, *109*(C4), doi:10.1029/2001JC001109.

Ono, N. (1968), Thermal properties of sea ice, IV, Thermal constants of sea ice, *Low Temp. Sci.*, *A26*, 329–349.

Ozbek, H., J. A. Fair, and S. L. Phillips (1977), Viscosity of aqueous sodium chloride solutions from $0-150^\circ$C, *Am. Chem. Soc. 29th Southeast Regional Meeting, Tampa, FL, November 9-11, 1971.*

Petrich, C., P. Langhorne, and Z. F. Sun (2006), Modelling the interrelationships between permeability, effective porosity and total porosity in sea ice, *Cold Reg. Sci. Technol.*, *44*(2), 131 – 144, doi:10.1016/j.coldregions.2005.10.001.

Table 1. Material parameters used in calculations

Parameter		Value (cgs units)	Reference[a]
Liquid heat capacity	c_l	4.0 J/cm^3/deg	*Weast* [1971]
Solid heat capacity	c_s	1.9 J/cm^3/deg	*Weast* [1971]
Liquid thermal conductivity	k_l	0.00523 J/s/cm/deg	*Lange and Forke* [1952]
Solid thermal conductivity	k_s	0.0214 J/s/cm/deg	*Slack* [1980]
Latent heat of solidification	L	306 J/cm^3	*Kerr et al.* [1990]
Gravitational acceleration	g	980 cm/s^2	
Kinematic viscosity	ν	0.018 cm^2/s	*Ozbek et al.* [1977]
Reference permeability	K_0	10^{-4} cm^2	*Freitag* [1999]
Saline density coefficient	β	7.5×10^{-4} 1/ppt	*Ruddick and Shirtcliffe* [1979]
Heat transfer coefficient	λ	0.12	*Wettlaufer et al.* [1997]

[a] Sometimes a measurement per unit mass has been converted to a one per unit volume. Many quantities vary with temperature but we have chosen a representative value.

Phillips, O. M. (1991), *Flow and Reactions in Permeable Rocks*, Cambridge University Press.

Pringle, D. J., H. Eicken, H. J. Trodahl, and L. G. E. Backstrom (2007), Thermal conductivity of landfast Antarctic and Arctic sea ice, *J. Geophys. Res.*, *112*(C4), doi:10.1029/2006JC003641.

Rees Jones, D. W. (2014), The convective desalination of sea ice, Ph.D. thesis, University of Cambridge, Cambridge, U. K.

Rees Jones, D. W., and M. G. Worster (2013a), Fluxes through steady chimneys in a mushy layer during binary alloy solidification, *J. Fluid Mech.*, *714*, 127–151, doi:10.1017/jfm.2012.462.

Rees Jones, D. W., and M. G. Worster (2013b), A simple dynamical model for gravity drainage of brine from growing sea ice, *Geophys. Res. Lett.*, *40*(2), 307–311, doi:10.1029/2012GL054301.

Ruddick, B., and T. Shirtcliffe (1979), Data for double diffusers: Physical properties of aqueous salt-sugar solutions, *Deep Sea Research Part A. Oceanographic Research Papers*, *26*(7), 775 – 787, doi:10.1016/0198-0149(79)90013-X.

Saenz, B. T., and K. R. Arrigo (2012), Simulation of a sea ice ecosystem using a hybrid model for slush layer desalination, *J. Geophys. Res.*, *117*(C5), C05,007, doi:10.1029/2011JC007544.

Schulze, T. P., and M. G. Worster (1998), A numerical investigation of steady convection in mushy layers during the directional solidification of binary alloys, *J. Fluid Mech.*, *356*, 199–220.

Slack, G. A. (1980), Thermal conductivity of ice, *Phys. Rev. B*, *22*, 3065–3071, doi:10.1103/PhysRevB.22.3065.

Turner, A. K., E. C. Hunke, and C. M. Bitz (2013), Two modes of sea-ice gravity drainage: A parameterization for large-scale modeling, *J. Geophys. Res.*, *118*(5), doi:10.1002/jgrc.20171.

Untersteiner, N. (1968), Natural desalination and equilibrium salinity profile of perennial sea ice, *J. Geophys. Res.*, *73*(4), 1251–1257.

Vancoppenolle, M., T. Fichefet, and C. M. Bitz (2005), On the sensitivity of undeformed Arctic sea ice to its vertical salinity profile, *Geophys. Res. Lett.*, *32*(16), doi:10.1029/2005GL023427.

Vancoppenolle, M., T. Fichefet, H. Goosse, S. Bouillon, G. Madec, and M. A. Morales Maqueda (2009a), Simulating the mass balance and salinity of Arctic and Antarctic sea ice. 1. Model description and validation, *Ocean Model.*, *27*(1—2), 33–53, doi:http://dx.doi.org/10.1016/j.ocemod.2008.10.005.

Vancoppenolle, M., T. Fichefet, and H. Goosse (2009b), Simulating the mass balance and salinity of Arctic and Antarctic sea ice. 2. Importance of sea ice salinity variations, *Ocean Model.*, *27*(1–2), 54–69, doi:10.1016/j.ocemod.2008.11.003.

Vancoppenolle, M., H. Goosse, A. de Montety, T. Fichefet, B. Tremblay, and J.-L. Tison (2010), Modeling brine and nutrient dynamics in Antarctic sea ice: The case of dissolved silica, *J. Geophys. Res.*, *115*(C2), doi:10.1029/2009JC005369.

Weast, R. C. (1971), *Handbook of Chemistry and Physics*, 52 ed., Chemical Rubber Co., Cleveland, OH.

Weeks, W. F. (2010), *On Sea Ice*, University of Alaska Press, Fairbanks, AK.

Wells, A. J., J. S. Wettlaufer, and S. A. Orszag (2010), Maximal potential energy transport: A variational principle for solidification problems, *Phys. Rev. Lett.*, *105*, 254,502.

Wells, A. J., J. S. Wettlaufer, and S. A. Orszag (2011), Brine fluxes from growing sea ice, *Geophys. Res. Lett.*, *38*(L04501), doi:10.1029/2010GL046288.

Wells, A. J., J. S. Wettlaufer, and S. A. Orszag (2013), Nonlinear mushy-layer convection with chimneys: stability and optimal solute fluxes, *J. Fluid Mech.*, *716*, 203–227, doi:10.1017/jfm.2012.541.

Wettlaufer, J. S., M. G. Worster, and H. E. Huppert (1997), Natural convection during solidification of an alloy from above with application to the evolution of sea ice, *J. Fluid Mech.*, *344*, 291–316.

Wettlaufer, J. S., M. G. Worster, and H. E. Huppert (2000), Solidification of leads: Theory, experiment, and field observations, *J. Geophys. Res.*, *105*(C1), 1123–1134, doi:10.1029/1999JC900269.

Whitman, W. G. (1926), Elimination of salt from sea-water ice, *Am. J. Sci. Ser. (5)*, *11*(62), 126–132, doi:10.2475/ajs.s5-11.62.126.

Widell, K., I. Fer, and P. M. Haugan (2006), Salt release from warming sea ice, *Geophys. Res. Lett.*, *33*(12), doi:10.1029/2006GL026262.

Worster, M. G. (1986), Solidification of an alloy from a cooled boundary, *J. Fluid Mech.*, *167*, 481–501, doi:10.1017/S0022112086002938.

Worster, M. G. (1992), Instabilities of the liquid and mushy regions during solidification of alloys, *J. Fluid Mech.*, *237*, 649–669.

Worster, M. G. (1997), Convection in mushy layers, *Ann. Rev. Fluid Mech.*, *29*(1), 91–122.

Worster, M. G. (2000), Solidification of fluids, in *Perspectives in Fluid Dynamics: a Collective Introduction to Current Research*, edited by G. K. Batchelor, H. K. Moffatt, and M. G. Worster, pp. 393–446, Cambridge University Press.

Zhu, J., A. Jabini, K. M. Golden, H. Eicken, and M. Morris (2006), A network model for fluid transport through sea ice, *Ann. Glaciol.*, *44*(1), 129–133.

Corresponding author: David W. Rees Jones, Atmospheric, Oceanic and Planetary Physics, Department of Physics, University of Oxford, Oxford, OX1 3PU, UK. (reesjones@atm.ox.ac.uk)

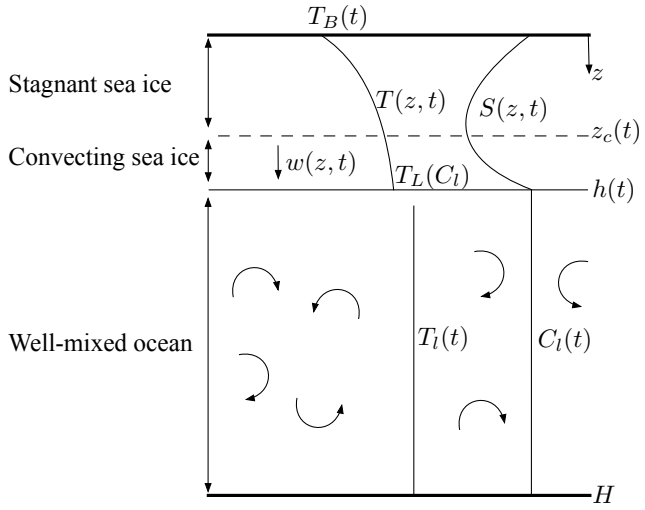

Figure 1. Schematic of the set-up considered in this article. The sea ice is divided into a stagnant layer and a convecting layer, as discussed in the text. Note that there is a thin thermal boundary layer (exaggerated) at the interface between the sea ice and the ocean (the purely liquid region) across which the modeled temperature field is discontinuous.

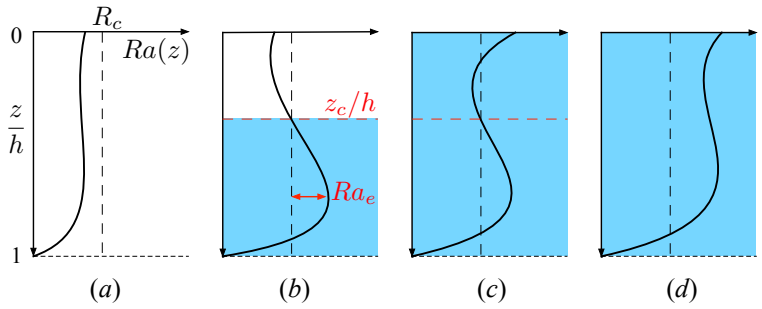

Figure 2. The convecting layer (shaded blue) with various types of local Rayleigh number profile. (a) No convection, since $Ra(z)$ is everywhere subcritical. (b) A lower layer convects. The effective Rayleigh number Ra_e is specified in equation (12) and used in equation (5). (c,d) Full-depth convection. We also investigated an alternative parameterization in which convection is confined below the dashed red line in (c).

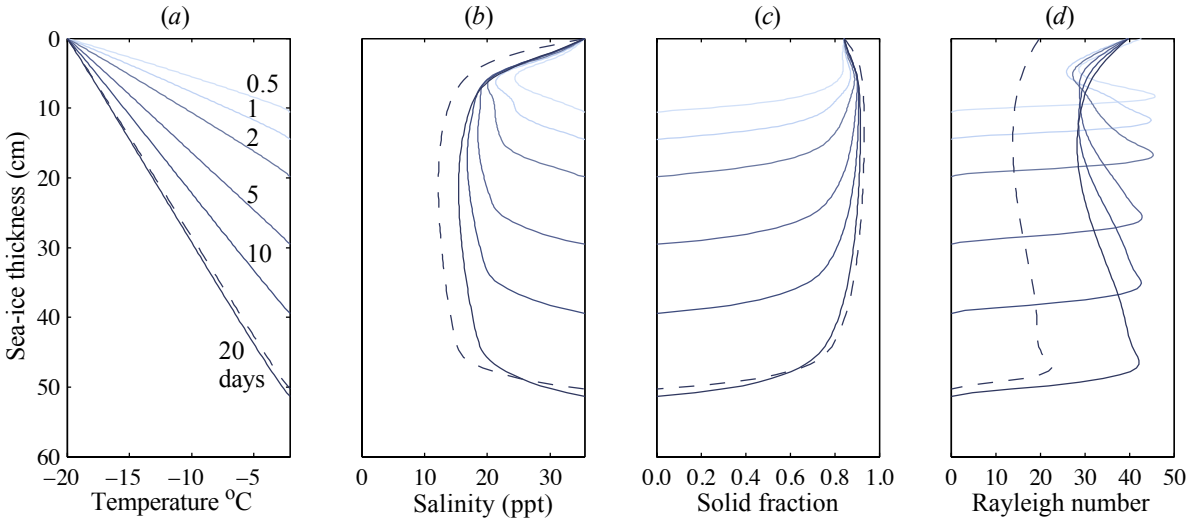

Figure 3. A series of profiles through the sea ice of (a) temperature, (b) salinity, (c) solid fraction and (d) local Rayleigh number. The calculations were performed for growth into a deep ocean with parameters $R_c = 40$ and $\alpha = 0.03$. The dashed curve gives profiles at the final time (20 days) at $R_c = 20$ and $\alpha = 0.03$.

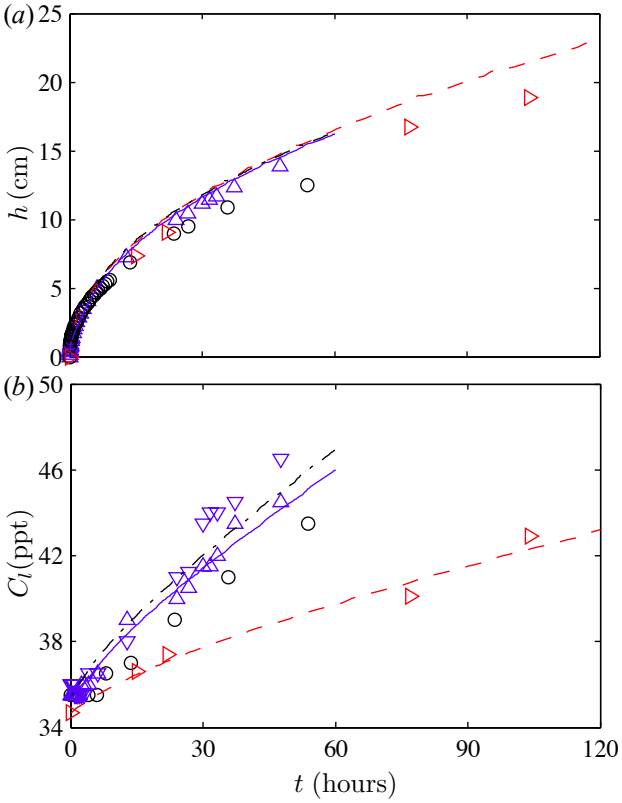

Figure 4. Experimental comparison in the case $T_B = -10°\mathrm{C}$: (*a*) sea-ice thickness and (*b*) ocean salinity measurements of *Wettlaufer et al.* [1997] (black circles), *Notz* [2005] (blue triangles; in (*b*) upward triangles correspond to samples from the middle of the tank, downward from the bottom, where it appears some ponding of more saline water may occur) and *Cox and Weeks* [1975] (red, right-pointing triangles). For reference, we show predictions of our model at $R_c = 20$ and $\alpha = 0.03$. The different depths of the tank $H = 37.6$, $H = 39.5$ and $H = 69$ cm (dot–dashed, solid, dashed), corresponding to the experiments above, give negligible differences in sea-ice thickness but significant ones in ocean salinity.

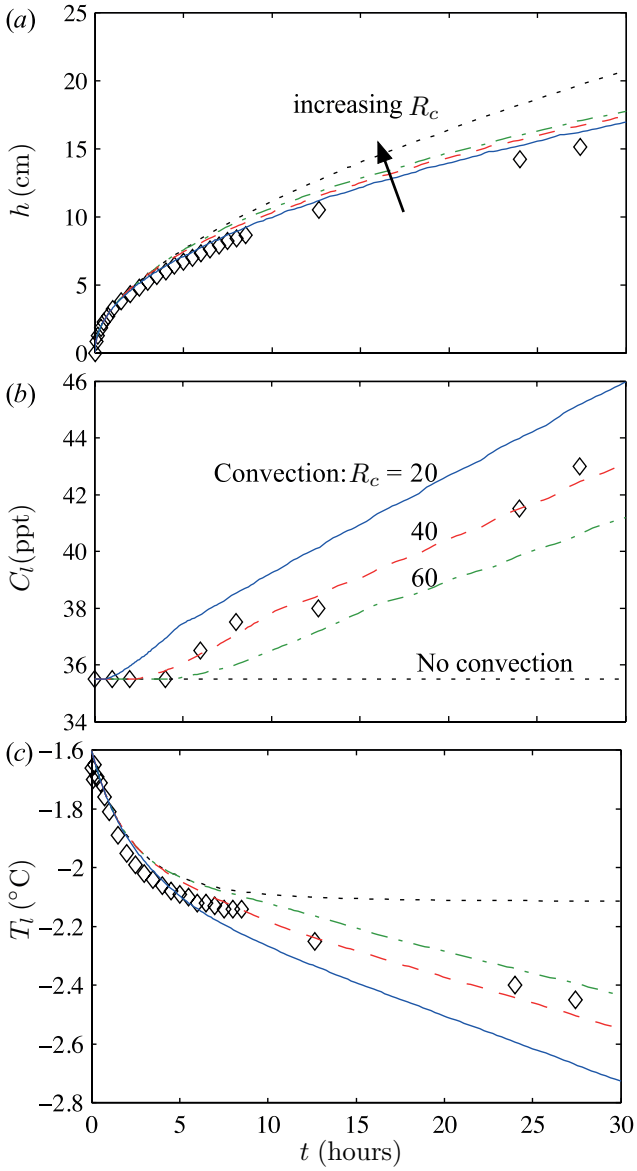

Figure 5. Results of our model at $T_B = -20°\mathrm{C}$: (a) sea-ice thickness, and (b) salinity and (c) temperature of the ocean. Open symbols are experimental measurements from *Wettlaufer et al.* [1997]. Calculations are run for the case of no convection ($R_c = \infty$) and for three different values of R_c (indicated in b), at fixed $\alpha = 0.03$. Experimental results for salinity of the ocean after 30 hours agree well with $R_c \approx 40$.

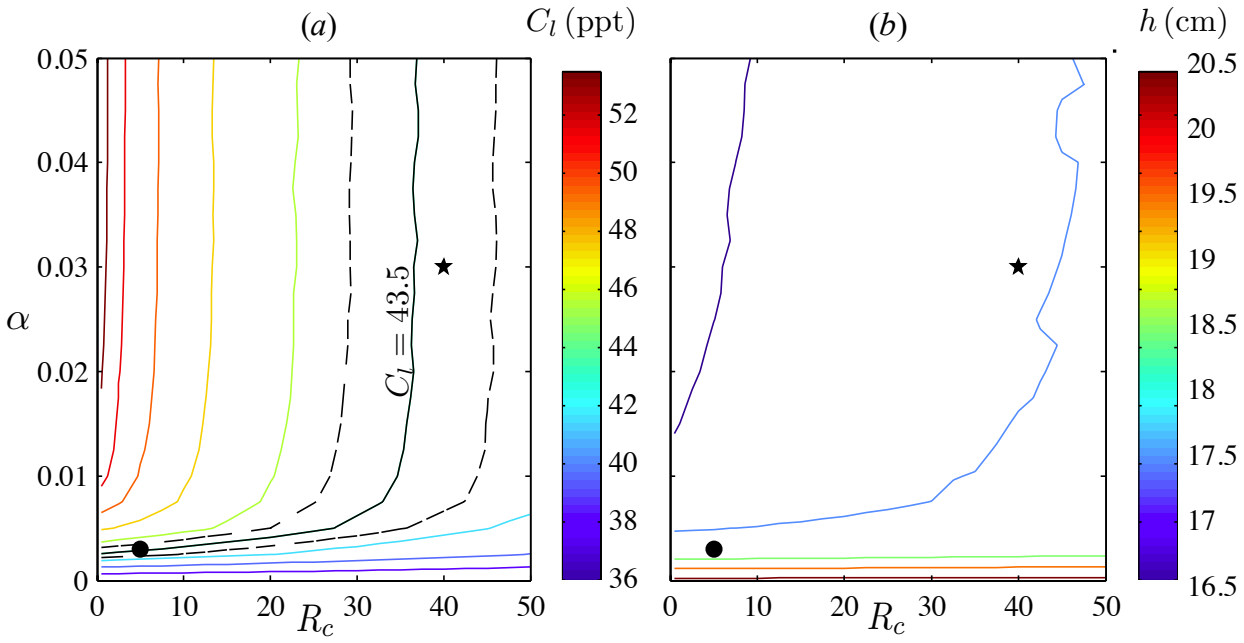

Figure 6. Model sensitivity to tuning parameters after $t = 30$ hours of sea-ice growth at $T_B = -20°$C. (a) Predicted ocean salinity in solid contours of 2 ppt from 35.5 increasing from bottom right to top left. The black dashed contours are at 42.5 and 44.5 ppt, and represent uncertainty about the experimentally observed value of 43.5 ppt (labelled). The high estimate is perhaps more likely given the bias towards underestimating the ocean salinity associated with the ponding and overflow discussed in section 3.1. (b) Predicted sea-ice thickness in contours of 1 cm from 16.5 cm increasing from top left to bottom right. Except perhaps at very small α, the thickness is largely insensitive to tuning parameters. The lack of smoothness of some of the contours is an insignificant consequence of the switches in the depth of the convecting layer, figure 7. The solid star ($R_c = 40, \alpha = 0.03$) is the main choice of tuning parameters used when comparing with the experiments of *Wettlaufer et al.* [1997]. In this region, the parameterization is insensitive to the value of α, as indicated by the approximately vertical contours. The solid circle ($R_c = 5, \alpha = 0.003$) is a possible alternative choice, consistent with observations sufficiently long after the onset of convection.

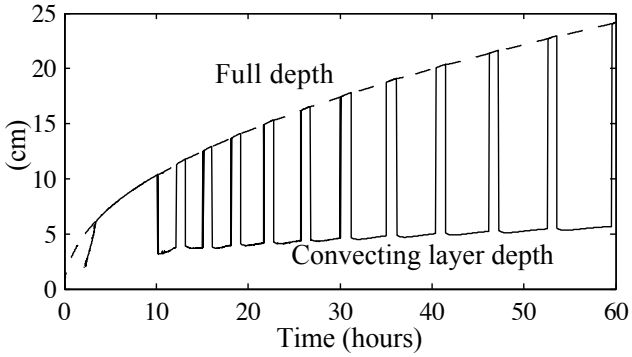

Figure 7. The depth of the convecting layer in the conditions described in figure 5 for parameters $R_c = 40$, $\alpha = 0.03$. The frequency of these cycles is dependent on α, which is not well constrained, but the behaviour is generic for sufficiently large α.

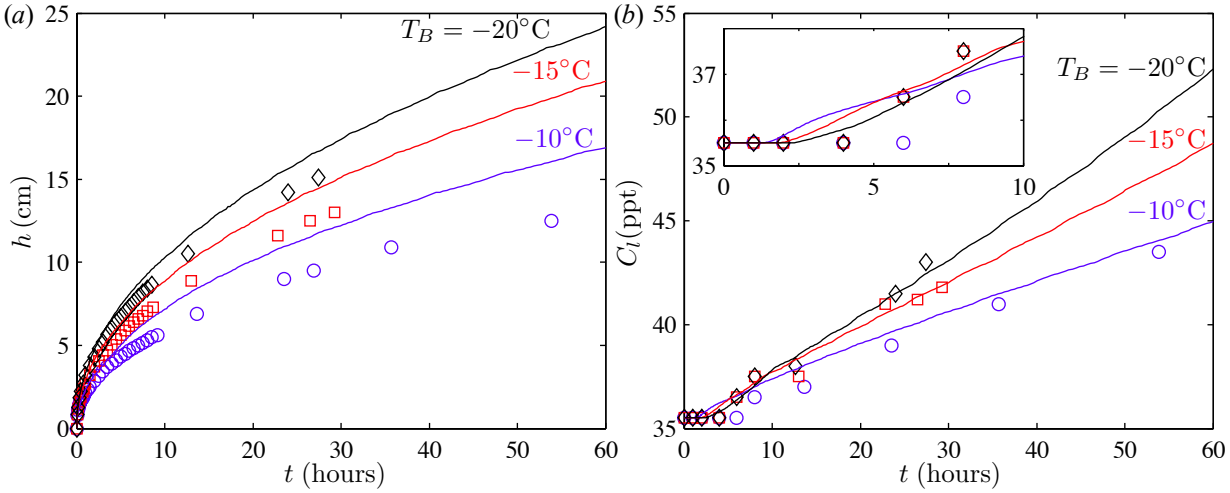

Figure 8. Model predictions of (a) sea-ice thickness and (b) ocean salinity at $R_c = 40$ and $\alpha = 0.03$ compared to the experiments of *Wettlaufer et al.* [1997] for $T_B = -20°C$ (diamonds), $T_B = -15°C$ (squares) and $T_B = -10°C$ (circles). The inset in (b) shows the onset of convection.

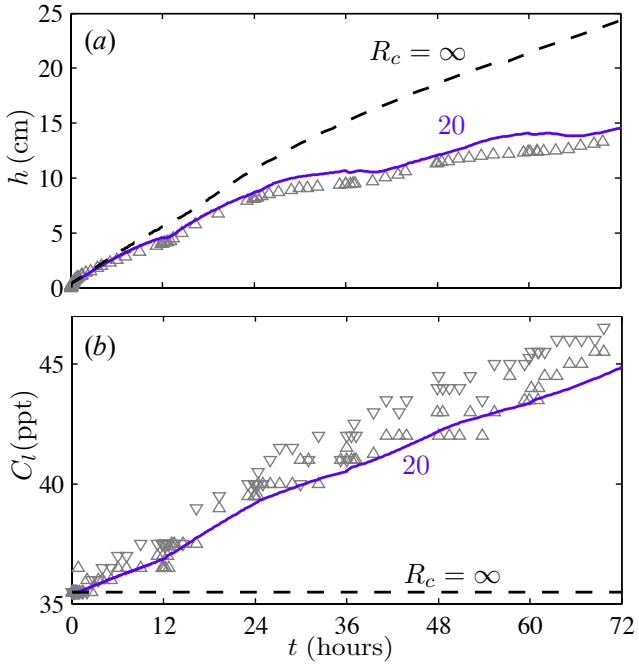

Figure 9. Experiment in which T_B is switched between $-5°C$ to $-10°C$ every twelve hours. Symbols are as in figure 4. The blue curve shows $R_c = 20$ and the black dashed curve shows $R_c = \infty$ (our model without convection).

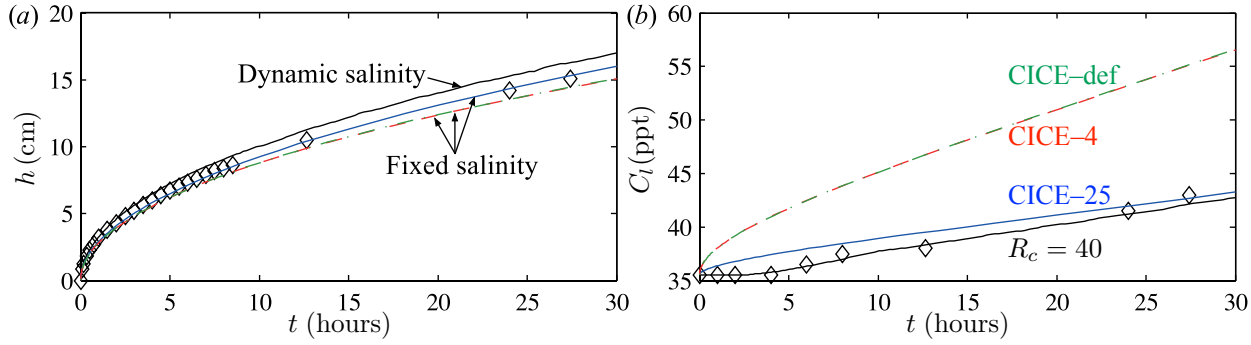

Figure 10. Experimental results of *Wettlaufer et al.* [1997] at fixed $T_B = -20°\mathrm{C}$ (diamonds) compared to predictions of our dynamic-salinity model (solid black curve) and fixed-salinity models at uniform CICE–25 (solid blue curve), CICE–4 (dashed red curve) and the default CICE–def (dot-dashed green curve).

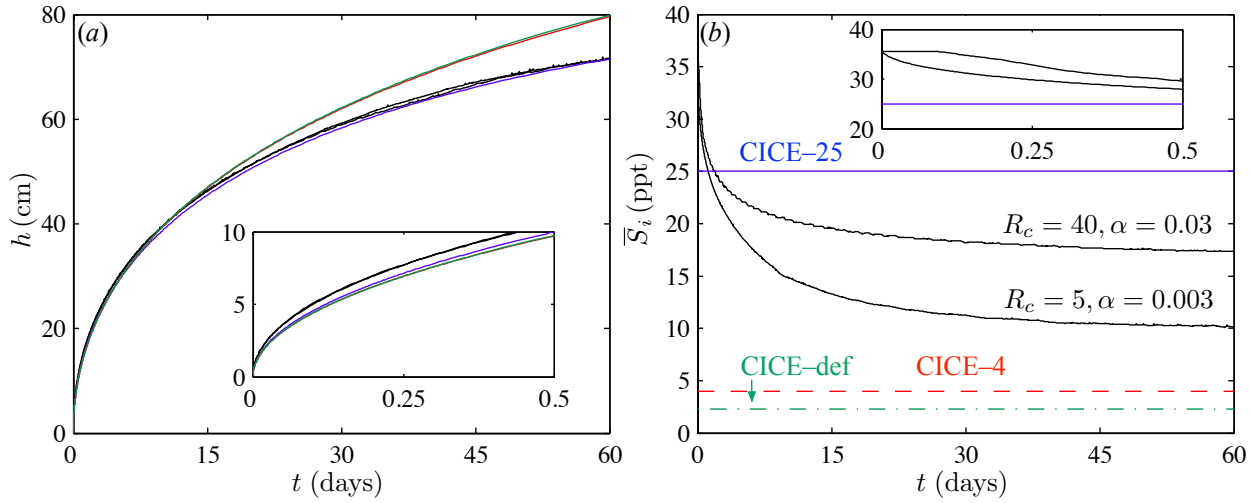

Figure 11. Comparison between fixed and dynamic-salinity models for a deep ocean at constant $T_B = -20°\mathrm{C}$, $T_l = -1.9°\mathrm{C}$ and $C_l = 35.5$ ppt. Note the much longer time scale than in previous figures. We include both the results for $R_c = 40$, $\alpha = 0.03$ and also the alternative parameterization $R_c = 5$, $\alpha = 0.003$ introduced in figure 6. The insets show initial 12 hours (0.5 days) including the delayed onset of convection in our dynamic-salinity model.

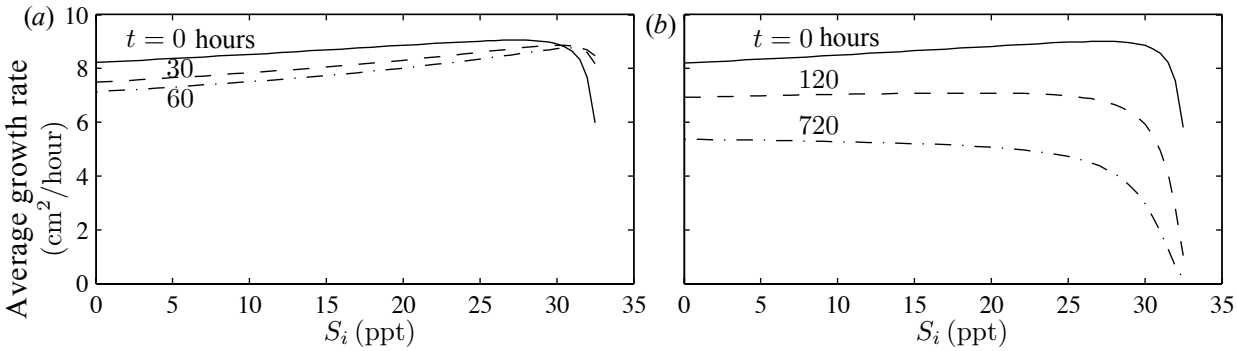

Figure 12. CICE calculation of sea-ice growth into (a) a tank of depth 37.6 cm and (b) a deep ocean with $T_B = -20^\circ$C as a function of prescribed, uniform ice salinity S_i. Motivated by our definition of 'exact diffusive growth', we plot the quantity h^2/t at various times. This quantity should be independent of time for diffusive growth. The growth rate decreases over time, although the common $t = 0$ curve would apply for all time if heat and salt fluxes to the ocean were neglected. The rapid decrease at large S_i is caused by the CICE expression for the thermal conductivity of ice dropping to zero (*cf.* equation (21) and discussion there).

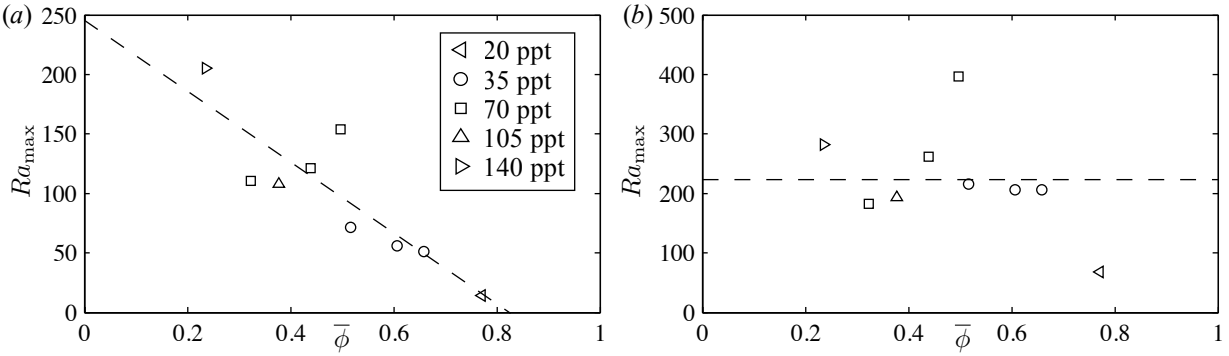

Figure 13. Maximum Rayleigh number $Ra_{\max}$ against mean solid fraction $\overline{\phi}$ for different initial salinities C_0 (see legend) calculated using our model on the experiments of *Wettlaufer et al.* [1997] using the methodology discussed in the text. We display the cases: (a) $K_l(\phi) = (1-\phi)^3$ and (b) $K_l(\phi) = (1-\phi)^2$. The dashed lines represent a linear and constant fit respectively. Note that the different scale on the $Ra_{\max}$ has no physical significance since any change could be incorporated in the reference permeability K_0 in equation (11).

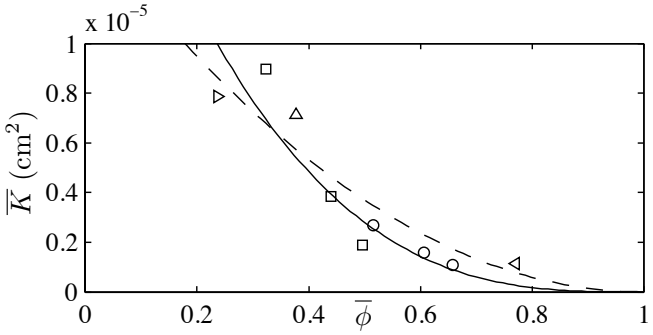

Figure 14. Bulk permeability inferred from the experiments of *Wettlaufer et al.* [1997] using equation (10) with a single bulk permeability $\overline{K}$ under the hypothesis that the onset of convection is determined by a critical bulk Rayleigh number $R_c = 40$. The legend is as in figure 13. The solid curve is a best fit cubic $\overline{K} = 2.24 \times 10^{-5}(1-\overline{\phi})^3$, which is perhaps a slightly better fit than the best fit quadratic $\overline{K} = 1.48 \times 10^{-5}(1-\overline{\phi})^2$, [*cf.* figure 7*b* in *Wettlaufer et al.*, 2000, for a complementary approach].

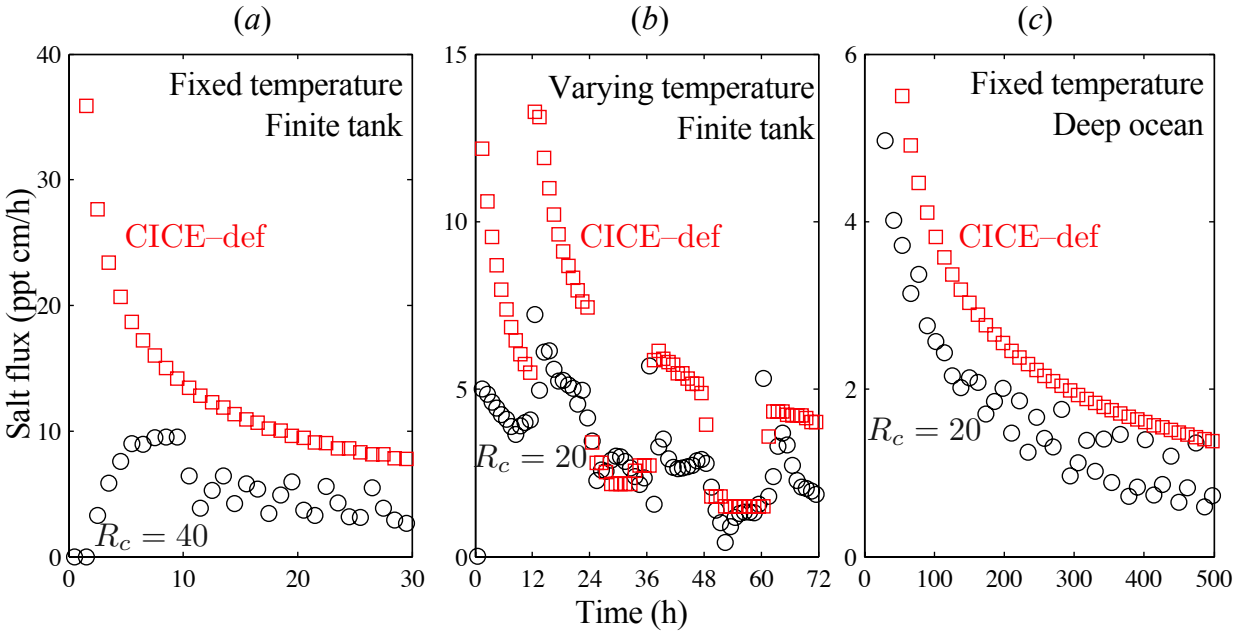

Figure 15. Comparison between a fixed-salinity (CICE-def, red squares) and our dynamic-salinity model (black circles) of predicted salt fluxes from sea ice. (*a* & *c*) provide an alternative interpretation of figures 10 & 11, respectively. (*b*) corresponds to the experiments in figure 9. We define the salt flux (relative to a reference salinity equal to the initial salinity of the ocean) as the rate of change with time of $(H-h)(C_l - C_0)$, or equivalently $h(C_0 - \overline{S}_i)$, and plot measurements averaged over an hour (*a*, *b*), and 12 hours (*c*). Note that the salt flux tends to infinity as t tends to zero for the CICE calculations and we have cropped this axis such that the first few points are removed to give a more reasonable scale for the rest of the measurements. The short-time variability in our model is usually associated with switches between full-depth and confined convection.